


RESEARCH ARTICLE

Reconciling different methods of high-latitude blocking detection

Evangelos Tyrlis¹  | Jürgen Bader^{1,2} | Elisa Manzini¹ | Daniela Matei¹¹Max Planck Institute for Meteorology, Hamburg, Germany²Uni Climate, Uni Research and the Bjerknes Centre for Climate Research, Bergen, Norway**Correspondence**

E. Tyrlis, Max Planck Institute for Meteorology, Bundesstrasse 53, Hamburg 20146, Germany.

Email: evangelos.tyrlis@mpimet.mpg.de

Funding information

German Federal Ministry of Education and Research European Union Horizon 2020, Grant/Award Numbers: FKZ 01LP1609A, 01LP2002A, GA 727852

Abstract

Blocking is associated with outbreaks of easterlies induced by a continuum of features including anticyclones, cyclones or both. Blocking identification methods disagree on the levels of high-latitude blocking (HLB) activity. We investigate the cause of the disagreement in HLB activity over the Northern Hemisphere obtained by two 2D methods: the PV- θ index and the Absolute Geopotential Height (AGH) reversal method. Although both classify as absolute field methods, the former yields nearly twice the winter HLB activity of the latter method. We show that this discrepancy is caused by the addition of a poleward criterion in the AGH method that requires strong poleward westerlies. The additional criterion in the AGH method shifts the focus on the detection of blocking ridges and thus other blocking circulation patterns are under-represented. Both methods agree on the climatology of midlatitude blocking because the poleward criterion has been tuned to capture the strong midlatitude blocking, but the discrepancy grows in high latitudes. HLBs are different because they occur on the northern flank of the westerlies and are associated with the equatorward displacement of the midlatitude jet. HLB anticyclones are weaker and do not induce strong poleward westerlies compared to their midlatitude counterparts. The implementation of a strict poleward criterion designed to identify midlatitude blocks rejects many HLBs. The use of the less strict cut-off threshold (CT) of $0 \text{ m } (^{\circ}\text{lat})^{-1}$ in the poleward criterion for latitudes higher than 60°N results in the convergence of climatology, interannual variability and trends of HLB between the two methods, especially during winter. The additional HLBs identified by the modified AGH algorithm develop from cyclonic wave breaking that is typical for oceanic blocking. The modified AGH method can be useful in detecting more robust HLB trends in climate model projections.

KEYWORDS

blocking, blocking index, Greenland blocking, Greenland ice melt 2019, high-latitude blocking

1 | INTRODUCTION

Atmospheric blocking is associated with the breakdown of the ‘high energy level’ state of the atmosphere, which is characterised by a strong midlatitude westerly jet, into a ‘low energy level’ state (Rex, 1950). When blocking occurs, the flow is dominated by a strong meridional component and the eastward progression of synoptic systems is obstructed. Blocking involves a wide range of circulation features that include a warm-cored blocking anticyclone, a cold-cored ‘blocking cyclone’ or both. Nevertheless, a number of prominent archetypal blocking patterns stand out from a continuous spectrum (e.g., Woollings *et al.*, 2018): (a) stationary ridges in large-amplitude Rossby waves, (b) Ω -blocks that feature a stronger anticyclonic centre, flanked by cut-off lows, and (c) dipole blocks in which cyclonic or anticyclonic wave breaking (Berrisford *et al.*, 2007; Tyrlis and Hoskins, 2008b) results in a configuration featuring an anticyclone over a cyclone, also referred to as a ‘Rex block’ (Berggren *et al.*, 1949; Rex, 1950). The disruption induced by blocking persists beyond synoptic time-scales and can instigate severe weather. Blocking anticyclones can cause droughts and heatwaves (Green, 1977; Black *et al.*, 2004; Trigo *et al.*, 2005; Dole *et al.*, 2011; Barriopedro *et al.*, 2011; Matsueda, 2011; Schneider *et al.*, 2012). Also, the diversion of synoptic activity by the block can bring heavy rain events in neighbouring locations (Webster *et al.*, 2011; Lau and Kim, 2012; Martius *et al.*, 2013; Lenggenhager *et al.*, 2019). During winter the anomalous easterly flow can result in extremely cold outbreaks (Sillmann and Croci-Maspoli, 2009; Buehler *et al.*, 2010; Bieli *et al.*, 2015; Whan *et al.*, 2016; Tyrlis *et al.*, 2019).

A universally accepted definition for blocking and a single theory that explains its dynamics of formation, maintenance and lysis, are still lacking (e.g., Tyrlis and Hoskins, 2008b; Nakamura and Huang, 2018; Woollings *et al.*, 2018; Nabizadeh *et al.*, 2019; Steinfeld and Pfahl, 2019). A plethora of blocking indices have been developed; each recognises different aspects of the phenomenon and yields often diverging climatologies of blocking action (e.g., Barriopedro *et al.*, 2010; Barnes *et al.*, 2012). They can be classified into three main categories: techniques that identify *field departures or anomalies*, others that look for reversals in *absolute fields*, and hybrid methods that combine both approaches (e.g., Barriopedro *et al.*, 2010; Dunn-Sigouin *et al.*, 2013). Field departure methods recognise blocking in areas of coherent and persistent anomalies of a variable that are typically observed in the vicinity of blocking ridges; they trace back to studies that identified blocking in areas of positive surface pressure anomalies (Elliott and Smith, 1949) or positive height anomalies (e.g., Charney *et al.*, 1981; Dole and Gordon, 1983; Shukla

and Mo, 1983; Knox and Hay, 1985; Dole, 1986). Other 2D fields, such as upper-level anticyclonic PV anomalies have been used to identify blocking ridges (Schwierz *et al.*, 2004). Field reversal methods stemmed directly from the property of blocking to drive the reversal of the usual midlatitude westerlies to easterlies (Rex, 1950). Treidl *et al.* (1981) and Tibaldi and Molteni (1990) identified large-scale and persistent easterly flow outbreaks over sectors that the meridional height gradient within the latitudinal band 40°–60°N becomes positive. Tibaldi and Molteni (1990) (hereafter TM90) added a second criterion that requires a significant westerly flow in the latitude band 60°–80°N. Blocking and outbreaks of easterly flow have been also identified in regions of large-scale and persistent reversals of the usual meridional gradient of θ on the 2 PVU (Potential Vorticity Unit) surface ($1 \text{ PVU} = 10^{-6} \text{ m}^2 \cdot \text{s}^{-1} \cdot \text{K} \cdot \text{kg}^{-1}$; Hoskins *et al.*, 1985), known as the dynamical tropopause (Pelly and Hoskins, 2003; Tyrlis and Hoskins, 2008a; 2008b; Woollings *et al.*, 2008; Masato *et al.*, 2009).

Field reversal methods combine succinctly a lot of information about the atmospheric flow into a single one-dimensional (1D) blocking index. However, prior knowledge of the mean atmospheric state is needed to compute an index along a Central Blocking Latitude (CBL) that corresponds to the jet stream where blocking is expected to occur. The uncertainties inherent to the 1D field reversal methods were alleviated with their application to 2D, a concept introduced by Berrisford *et al.* (2007), further developed by Masato *et al.* (2013b) and expanded to height reversals by Scherrer *et al.* (2006) and Davini *et al.* (2012) (hereafter D12). Masato *et al.* (2013b) developed an analogue to the 2D PV– θ blocking index that has 500 hPa geopotential height as an input. D12 retained the criterion introduced by TM90 ensuring that an easterly flow is identified equatorward of a location while a westerly flow of appreciable strength should be found to its north (Equation 3 below). With the addition of the criterion, both the algorithms by TM90 and D12 actually identify anticyclonic centres and not only regions of easterly outbreaks. Thus, they resemble the departure field methods in their propensity to identify blocking highs, which, as mentioned above, is one of the ‘blocking elements’. This adaptation results in algorithms that focus on the detection of blocking in the presence of ridges and puts less emphasis on other blocking circulation patterns. However, the classification of blocking episodes (BEs) according to the intensity of the warm and cold air-mass extrusions revealed that both the warm anticyclone to the north and cold cyclone to the south are important elements for the blocking formation and thus they should be equally favoured in a blocking diagnostic method (Masato *et al.*, 2012; 2013a). On the other hand, the 2D methods that are based on

the PV- θ index retained the even detection of blocking across the whole spectrum of circulation patterns, which is inherent to absolute field methods, and adhered to the original notion of blocking as acting to reverse the westerlies.

When a block is actually blocking the jet, then the westerlies can shift either northwards or southwards (or split) and the direction may be irrelevant but frequently depends on the region and season. For High-Latitude Blocking (HLB), which occurs on the northern flank of the westerlies, it is the southward distortion of the westerlies that really matters, not whether any westerlies are found to the north. High-latitude blocks are weaker than their mid-latitude counterparts (e.g., figure 4a in D12; Woollings *et al.*, 2008) but they are not deprived of dynamical significance. The negative (positive) phase of the North Atlantic Oscillation has been envisaged as describing a period of frequent (infrequent) HLB over the Atlantic. A similar relationship holds for HLB over the Pacific and the West Pacific Pattern (Woollings *et al.*, 2008). Blocking provides a useful framework for studying stratosphere-troposphere coupling (Nishii *et al.*, 2011; Davini *et al.*, 2014; Huang *et al.*, 2017). Stratospheric warmings are often preceded by HLB (Martius *et al.*, 2009; Peings, 2019; Tyrlis *et al.*, 2019; White *et al.*, 2019) but also episodes of weakening of the stratospheric polar vortex can cause surface high-impact weather patterns, such cold extremes, which often occur in the presence of high- or midlatitude blocking (Kostad *et al.*, 2010; Woollings *et al.*, 2010; Lehtonen and Karpechko, 2016; Garfinkel *et al.*, 2017; Kretschmer *et al.*, 2018; King *et al.*, 2019).

Recently, blocking has been placed at the core of a difficult conundrum concerning the possibility of a link between Arctic Amplification (e.g., Serreze and Francis, 2006) and more frequent cold surges in midlatitudes (e.g., Cohen *et al.*, 2020). Previous studies presented conflicting evidence for a recent upward trend in blocking activity caused by Arctic Amplification (Francis and Vavrus, 2012; Barnes, 2013; Barnes *et al.*, 2014; Francis and Vavrus, 2015). The recent increase in frequency and persistence of Ural blocking, which is a key driver of the Warm Arctic-Cold Siberia pattern (Mori *et al.*, 2014; 2019), are often attributed to the warming and sea-ice decline over the Barents-Kara Seas emerging after the late 1990s (Luo *et al.*, 2016; 2017; 2019; Yao *et al.*, 2017). The feedback of Ural blocking on enhancing Arctic sea-ice loss has also been investigated (Gong and Luo, 2017; Chen *et al.*, 2018; Tyrlis *et al.*, 2020). Furthermore, episodes of Arctic anticyclones, which often can be categorised as HLB, have been found to be important drivers of the summertime Arctic sea-ice melting (e.g., Ogi and Wallace, 2012; Ding *et al.*, 2017; Papritz and Wernli, 2018). In particular, the role of Greenland blocking in driving

summertime melting of Greenland ice has been found to be of paramount importance (e.g., Ballinger *et al.*, 2018; Wang *et al.*, 2019)

Despite the significance of HLB, there is poor agreement among blocking indices in their ability to capture its frequency of occurrence. Here, we revise the poleward criterion used in D12 and we show that the discrepancy is due to the very strict poleward criterion that neglects many HLB episodes. The proposed modified algorithm leads to a convergence with the climatology produced by the PV- θ blocking index, it provides a more complete identification of HLB, and thus it can be very useful for future studies of the HLB phenomenon. Admittedly, each method is characterised by its own limitations and no method can be perceived as the panacea for blocking identification. However, the resulting convergence between methods can be seen only as having a beneficial impact in improving HLB identification. In addition, the proposed modified algorithm can be used for the improved identification of HLB in the cases that the standard model output does not include the required input variables to the PV- θ blocking index and thus computationally expensive pre-processing is required. In Section 2 we describe the two methods employed by this study to recognise Northern Hemisphere blocking and we highlight the necessity for implementing a less strict poleward criterion compared to the one employed by D12 which is better tuned for identifying HLB. In Section 3 we show that the modified algorithm yields a HLB climatology that agrees with the one produced by the PV- θ blocking index. In Section 4, we confirm that the additional days of HLB episodes that are recognised by the implementation of the modified algorithm feature a typical blocking signature. Also, we present the case-study of Greenland blocking in spring 2019 when the modified algorithm significantly improved blocking diagnosis over the region. Then in Section 5 we show that the modified algorithm yields interannual variability and trends of HLB that closely agree with those produced by the PV- θ blocking index. Finally, Section 6 summarizes the results and draws conclusions.

2 | DATA AND METHODS

2.1 | Data and blocking identification methods

We diagnose blocking based on variables from the ERA-Interim dataset (Dee *et al.*, 2011) that covers the period January 1979–August 2019. These include geopotential height at 500 hPa and potential temperature (θ) on the 2PVU surface. Blocking is identified with two prominent absolute field methods. The first method, which

will be referred to as the 2D PV– θ blocking index, is the algorithm used in Tyrlis *et al.* (2015; 2019; 2020). This algorithm is an expansion of the 1D PV– θ blocking index, which was introduced by Pelly and Hoskins (2003) and subsequently used by Tyrlis and Hoskins (2008a; 2008b) and Masato *et al.* (2012; 2013a), to two dimensions. The original 1D PV– θ blocking index distinguishes blocking along a CBL determined as the location of the maximum in latitude of the 300 hPa synoptic time-scale transient eddy energy. It looks for areas of wave breaking that leads to reversals of the climatological meridional gradient of θ in the vicinity of the dynamical tropopause. In the Northern Hemisphere, the dynamical tropopause is represented by the 2 PVU surface (e.g., Hoskins *et al.*, 1985) over the mid-latitudes. In the original 1D PV– θ blocking index, local and instantaneous blocking is identified at grid-points along the CBL where the blocking index is positive. Large-scale blocking is identified where local and instantaneous blocking extends over a sector of at least 15° in longitude. A *blocking event* is then defined at a specific longitude when large-scale blocking is identified within 10° in longitude. A blocking event is referred to as a *blocking episode* (BE) if it lasts for 5 days or longer. The 2D algorithm used in this study follows Berrisford *et al.* (2007) and Woollings *et al.* (2008) in allowing CBL to vary within the latitude band $25\text{--}73^\circ\text{N}$ at increments of 4° latitude. In this sense the uncertainties in blocking identification based on the 1D definition due to the seasonal variation of the CBL are alleviated (see also Barnes *et al.*, 2012) and also the identification of HLB is allowed. Finally, we identify BEs on a 5° longitude by 4° latitude grid that extends over the latitudinal band $25\text{--}73^\circ\text{N}$.

The second method to identify blocking is the bi-dimensional method introduced by D12. To identify instantaneous blocking at a grid-point with longitude λ_O and latitude ϕ_O , the meridional gradient of geopotential height to the north *GHGN* and south *GHGS* of the specific grid-point are calculated as follows:

$$GHGS(\lambda_O, \phi_O) = \frac{Z_{500}(\lambda_O, \phi_O) - Z_{500}(\lambda_O, \phi_S)}{\phi_O - \phi_S}, \quad (1)$$

$$GHGN(\lambda_O, \phi_O) = \frac{Z_{500}(\lambda_O, \phi_N) - Z_{500}(\lambda_O, \phi_O)}{\phi_N - \phi_O}, \quad (2)$$

where ϕ_O ranges from 30 to 75°N and λ_O from 0 to 360°E , both at increments of 2.5° longitude or latitude; $\phi_N = \phi_O + 15^\circ$ and $\phi_S = \phi_O - 15^\circ$.

Instantaneous Blocking at a specific grid-point with coordinates λ_O, ϕ_O is identified when

$$GHGS(\lambda_O, \phi_O) > 0 \text{ and } GHGN(\lambda_O, \phi_O) < -10 \text{ m } (^\circ\text{lat})^{-1}. \quad (3)$$

The first criterion of Equation (3) ensures that easterly flow is identified on the equatorward side of the grid-point, while the second criterion requires that a westerly flow of appreciable strength is found on its poleward side, thus a blocking ridge is distinguished. Hereafter, we will refer to these as the equatorward and poleward criteria, respectively. The value of the Cut-off Threshold (CT) for the poleward criterion corresponds to the threshold used. D12 used the threshold value of $-10 \text{ m } (^\circ\text{lat})^{-1}$. In this study, various values of the CT are used with view to evaluate the method for a more effective identification of HLB. Here, the term HLB refers mainly to BEs identified polewards of 60°N . Also, we refer to the original algorithm employed by D12 as AGH (Absolute Gradient Height). The notation of the modified AGH algorithm set-ups used in this study is described in Table 1. In the case that various values of the CT are applied throughout the Northern Hemisphere, we refer to these set-ups as AGH_m. For example, in the case that $\text{CT} = -5 \text{ m } (^\circ\text{lat})^{-1}$ is applied everywhere, we label this set-up as AGH_m-5 and accordingly for other values. We refer to the algorithm with a $\text{CT} = 0 \text{ m } (^\circ\text{lat})^{-1}$ applied only for high latitudes ($\geq 60^\circ\text{N}$) but $\text{CT} = -10 \text{ m } (^\circ\text{lat})^{-1}$ elsewhere as AGH_h0. To account for a less abrupt change in the CT, in the algorithm set-up AGH_h0*, an intermediate value of $-5 \text{ m } (^\circ\text{lat})^{-1}$ in the latitude band of $55\text{--}65^\circ\text{N}$ is applied.

$$GHGS2(\lambda_O, \phi_O) = \frac{Z_{500}(\lambda_O, \phi_S) - Z_{500}(\lambda_O, \phi_S - 15^\circ)}{15^\circ}, \quad (4)$$

$$GHGS2(\lambda_O, \phi_O) < -5 \text{ m } (^\circ\text{lat})^{-1}. \quad (5)$$

Note that in D12 a third meridional gradient of geopotential height (*GHGS2*) is calculated between 15° and 30° south of the specific grid-point where blocking is evaluated (Equation 4). The application of a third criterion (Equation 5) is employed to exclude Low-Latitude Blocks (LLBs) from the analysis, which are manifested in the form of a northward shift of the subtropical easterlies. Essentially, this additional criterion requires that a band of westerlies must be present in the latitudinal band between 15° and 30° south of the grid-point where blocking is evaluated. This criterion has been employed in D12 but suppressed in most subsequent studies (e.g., Davini *et al.*, 2017; Athanasiadis *et al.*, 2020; Schiemann *et al.*, 2020, and references therein) which were based on the algorithm described in D12 or the very similar one introduced by Scherrer *et al.* (2006). Therefore for our results to be compatible and comparable with those from previous studies that employed the same blocking detection scheme, and because the focus of this study is on HLB, we did not include in our algorithm the third criterion introduced by D12. Nevertheless, for completeness, in Section 3 we

TABLE 1 Notation of the modified versions of the AGH algorithm

Algorithm modification	Acronym	Cut-off threshold CT (m (°lat) ⁻¹)		
Everywhere		30°N ≤ φ ₀ ≤ 75°N		
	AGH_m-10	-10		
	AGH_m-5	-5		
High latitudes	AGH_m0	0		
		30°N ≤ φ ₀ < 60°N	60°N ≤ φ ₀ ≤ 75°N	
	AGH_h0	-10	0	
High latitudes*		30°N ≤ φ ₀ < 55°N	55°N ≤ φ ₀ < 65°N	65°N ≤ φ ₀ ≤ 75°N
	AGH_h0*	-10	-5	0

Note: The first rows list algorithm set-ups of the class AGH_m in which a CT is applied throughout the Northern Hemisphere. Various values of CT in the range -10 to 1 m (°lat)⁻¹ are employed in this study (e.g., Figure 6). The second row describes the algorithm set-up AGH_h0 in which CT = 0 m (°lat)⁻¹ is applied only for high latitudes but CT = -10 m (°lat)⁻¹ elsewhere. In the third row, a variation of the previous set-up is described that accounts for a less abrupt change in the CT (AGH_h0*) in which an intermediate value of -5 m (°lat)⁻¹ in the latitude band 55–65°N is applied (Figure S7).

provide supplementary analysis that elucidates the impact of the addition of the third criterion on the blocking frequency over the Northern Hemisphere.

In fact, the blocking algorithm introduced by D12 without the implementation of their third criterion is equivalent to the algorithm noted here as AGH_m-10. A grid-point is associated with large-scale blocking in the case that both criteria of Equation (3) are satisfied for a continuous sector larger than 15° in longitude. A BE is detected with this method when large-scale blocking is occurring somewhere within a box region of size 5° latitude by 10° longitude centred on that grid-point continuously for at least 5 days. Note that blocking with this method is evaluated on a different grid compared to the PV-θ blocking index; it is a 2.5° longitude by 2.5° latitude grid that extends over the latitudinal band 30–75°N.

In Section 5 we calculate trends over the period 1991–2014 (Figure 15 below), which has been commonly used in previous studies (e.g., Sun *et al.*, 2016) to investigate the key drivers of the cooling over central Asia occurring simultaneously with a pronounced Warm Arctic–Cold Siberia pattern. Here we use this period as a benchmark to calculate blocking activity trends with view to assessing the comparative importance of the blocking identification method. The statistical significance of linear trends is evaluated with a two-sided *t*-test. The statistical significance of the anomalous fields, which correspond to the composite mean signature of the new BE days identified after a step-wise change in the value of the CT (Figures 7–9 below and Figure S8) is assessed with a Monte Carlo method. The same number of wintertime days, as the one of new BE days identified by the modified blocking identification algorithm over a selected region, is randomly sampled during 1979–2019. This process is repeated 1,000 times and a synthetic distribution of artificially constructed anomalies

captures the expected winter variability for a same-size sample. In the case that the observed composite mean anomaly of the new BE days at a given grid-point ranks in the upper or lower 2.5% of the synthetic distribution of samples generated by the Monte Carlo process, then the anomaly is deemed as statistically significant at the 95% confidence level.

2.2 | Need for a modification of the blocking index criteria

The cut-off threshold of -10 m (°lat)⁻¹ was originally employed by the 1D algorithm in TM90 to identify midlatitude blocking in the vicinity of 60°N. Assuming geostrophic balance, this threshold is equivalent to 8 m s⁻¹ in midlatitudes (Barnes *et al.*, 2012). This choice was dictated by the early empirical studies on midlatitude blocking and the associated bifurcation of the westerlies into two distinctive branches with the poleward branch of the jet being of appreciable strength. The threshold was later employed unmodified by Scherrer *et al.* (2006) and D12 without further calibration to recognise blocking over the whole Northern Hemisphere. However, HLB is mostly associated with a southward displacement of the westerlies and in most cases the employment of a strict poleward criterion may not be appropriate for the identification of blocking there. Indeed, Masato *et al.* (2013b) raised concerns over the substantial reduction in HLB occurrence due to the application of the poleward criterion in TM90, in comparison to other studies that employed the PV-θ blocking index (Woollings *et al.*, 2008; Masato *et al.*, 2013a).

The cumulative probability of winter days for which the poleward criterion is fulfilled is much higher than 70% for locations along the midlatitude westerlies (Figure 1a).

This probability is lower during transitional seasons and mainly summer (Figures S1, S2 and S3) when the westerlies over the Northern Hemisphere weaken. Thus, the cut-off threshold can be frequently surpassed in midlatitudes and blocking can be detected by the AGH algorithm. Indeed the zonal westerly flow in the mid-troposphere is much higher than $8 \text{ m}\cdot\text{s}^{-1}$ over these regions (Figure S4). Regions of high values of cumulative probability or strong westerlies stretch polewards at the exits of the North Pacific and Atlantic midlatitude jets where actually midlatitude blocking preferentially occurs (e.g., Woollings *et al.*, 2018). Occasional midlatitude blocking action over the eastern Atlantic, Europe, western Russia and the eastern Pacific leads to the poleward displacement of the westerlies. Therefore, it is not a coincidence that the CT in TM90 was calibrated to recognise exactly these blocking conditions. However, northwards of 60°N , the poleward criterion is satisfied for less than 30% of the winter days. In particular, over Greenland and in the vicinity of the Bering Strait, this probability can be as low as 10% (Figure 1a). The poleward criterion may indeed be too strict there; by construction many days associated with BE may be excluded. When the CT is relaxed gradually to $0 \text{ m}(\text{°lat})^{-1}$, the cumulative frequency of winter days for which the criterion is fulfilled increases substantially over high latitudes (Figure 1b,c,d).

The Probability Distribution Function (PDF) of the winter height gradient calculated just polewards of locations over Greenland and Far East Asia are significantly shifted towards higher values (weaker westerlies) compared to those over Europe and the Urals (Figure 1d). While the cut-off threshold of $-10 \text{ m}(\text{°lat})^{-1}$ marks the peaks of the PDFs for Europe and the Urals, it marks the lower tail of the PDFs for Greenland and the Bering Strait. Given that the westerly flow is weaker over high latitudes, for an algorithm to allow the identification of conditions associated with blocking on a fair basis over both middle and high latitudes, different thresholds should be employed. Consequently, a CT closer to $0 \text{ m}(\text{°lat})^{-1}$ can be more suitable for identifying winter blocking in high latitude locations (Figure 1d) to allow for more blocking days to be included. Therefore employing a criterion that requires at least a weak westerly flow to the north of the grid-point under investigation appears to be a more realistic parametrization for HLB identification over regions where a strong westerly jet is not so common (Figure S4). Also, conceptually, there is a continuum in the strength of anomalies associated with HLBs; the ones at very high latitudes tend to be weak and correspond to very weak reversals of the meridional gradient. Only some events further south are associated with anomalies that can be compared in amplitude to their midlatitude counterparts (Woollings *et al.*, 2008). Thus, the weaker anticyclones associated with

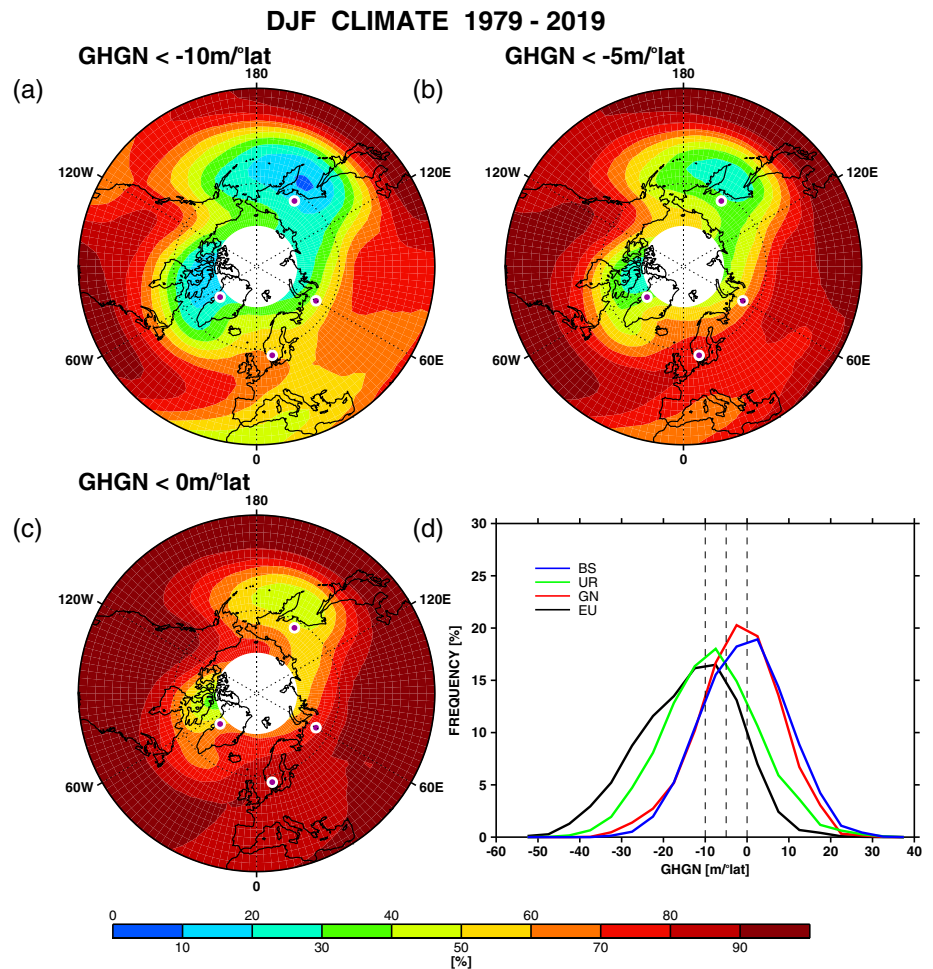
HLB (also Section 4.1) can only induce a weaker westerly flow on their poleward side. Consequently, the poleward criterion should be adapted to the weaker signature of HLB and become less strict. Lastly, during the transitional seasons, the differences in the PDFs between high and lower latitude regions are very similar to these for winter (Figures S2d and S3d) while during the summer the differences dampen (Figure S1d). To ensure simplicity in the algorithm, the same cut-off threshold should be used to identify blocking in high latitudes throughout the year.

3 | CHANGES IN BLOCKING CLIMATOLOGY

We compare the climatology of BE frequency over the Northern Hemisphere acquired by the 2D PV- θ blocking index to those obtained with the use of AGH algorithm and its modified versions for various cut-off thresholds of the poleward criterion. The unmodified AGH algorithm yields a winter-mean BE frequency (Figure 2c) which closely agrees with previous studies (e.g., Davini *et al.*, 2012; Woollings *et al.*, 2018). It recognises the salient features of midlatitude blocking action over the eastern Atlantic, Europe and its extension towards the Ural Mountain range, and the Pacific sector. However, the blocking activity is everywhere lower than the climatology acquired by the PV- θ blocking index (Figure 2a). Specifically, over Europe the difference is approximately 3–4% but significantly grows in the hot-spots of blocking activity over Greenland and the Bering Strait, where more than double blocking activity is recognised by the PV- θ blocking index (Figure 2a). The European maximum of BE frequency identified by the PV- θ algorithm is shifted southwards by up to 10°lat compared to that obtained by the AGH algorithm. The latter index has the propensity to identify the location of the blocking high whereas the PV- θ blocking index identifies the regions of easterly flow outbreaks, which lie to the south of the blocking highs (see also subsequent Figure S12). Areas of high winter BE frequency in the Subtropics are present in Figure 2c, but eliminated when the third criterion (Equation 5) is applied (Figure S5).

Consistent with D12, these LLBs, which are associated with a northward shift of the subtropical easterlies, are totally excluded to the south of $40\text{--}45^\circ\text{N}$ when this additional criterion is applied not only during winter but also in boreal summer and transitional seasons (not shown). Blocking activity is slightly reduced over the mid and high latitudes but the hemispheric pattern remains unaltered. The reduction is locally larger than 10% in the vicinity of the Laptev and East Siberian Seas. We constructed composite mean height anomalies by including all the winter

FIGURE 1 Cumulative frequency of winter (DJF) days for which the poleward criterion (second criterion in Equation 3) is satisfied for cut-off thresholds (a) $CT = -10 \text{ m } (^\circ\text{lat})^{-1}$, (b) $CT = -5 \text{ m } (^\circ\text{lat})^{-1}$ and (c) $CT = 0 \text{ m } (^\circ\text{lat})^{-1}$. Essentially, this corresponds to the percentage of winter days for which the westerly zonal flow is stronger than these various thresholds to the north of the chosen grid point (Geopotential Height Gradient North, GHGN). The relaxation of the threshold allows a larger number of winter days with weaker westerly flow to be included. This is further exemplified by the histograms shown in (d) that illustrate the percentage of winter days associated with a certain GHGN at 500 hPa (bin interval is $5 \text{ m } (^\circ\text{lat})^{-1}$) calculated to the north of four representative grid-points in Greenland (red), Europe (black), Urals (green) and near the Bering Strait (blue). These grid-points are also marked in (a–c). Vertical dashed lines mark the above mentioned CTs. Note that the cumulative percentages on the left side of these thresholds correspond to the cumulative frequencies in (a–c)



HLB days eliminated after the addition of the third criterion in the AGH_h0 algorithm. A typical blocking signature was clearly identified for HLB over Greenland and the Bering Strait (not shown). The addition of the third criterion requires that local and instantaneous blocking is identified at a grid-point when easterlies are found to its south but also encompassed by westerlies to its north, as well as in the band $15\text{--}30^\circ$ latitude to its south (Equations 3 and 5). This combination of criteria deviates from the traditional definitions because it puts a geometric constraint of around 15° latitude in the width of the detected easterlies so that local and instantaneous blocking is identified at the specific grid-point. Eventually, this extra restriction can lead to the reduction of the days identified as BE. The advantage of the third criterion in filtering out LLBs does not outweigh the incorrect elimination of HLB, in particular because the correct detection of which is the main topic of this study. Therefore, we suggest that potential application of the third criterion should be restricted to the south of $40\text{--}45^\circ\text{N}$. Also, the importance of the exact choice of the cut-off threshold of the criterion in Equation 5 could be a subject of further research but falls outside the scope

of this work which focuses on HLB. LLBs are filtered out by the $PV\text{--}\theta$ blocking index because, unlike in TM90 and D12, this index is calculated as the difference of θ on the 2 PVU surface averaged over box regions of significant latitudinal extent which can smooth out the weaker easterly outbreaks in the Subtropics (Masato *et al.*, 2013b).

Higher occurrence of winter HLB was also reported by other studies that employed various versions of the 2D $PV\text{--}\theta$ blocking index in the Northern or Southern Hemisphere (e.g., Berrisford *et al.*, 2007; Woollings *et al.*, 2008), but also by studies that recognised blocking in areas of reversals of the usual meridional gradient of geopotential height at 500 hPa (e.g., Masato *et al.*, 2013a; 2013b). The disagreement with the results by D12 is therefore not due to the different variable utilised by each algorithm or probably differences in the blocking dynamics (upper- versus mid-tropospheric levels) captured by each method. It is worth noting that a very high frequency of HLB was also reported by other studies (e.g., Croci-Maspoli *et al.*, 2007), which looked for blocking episodes in areas of persistent and strong anticyclonic PV anomalies in the vicinity of the tropopause. The modified algorithm AGH_h0 yields a

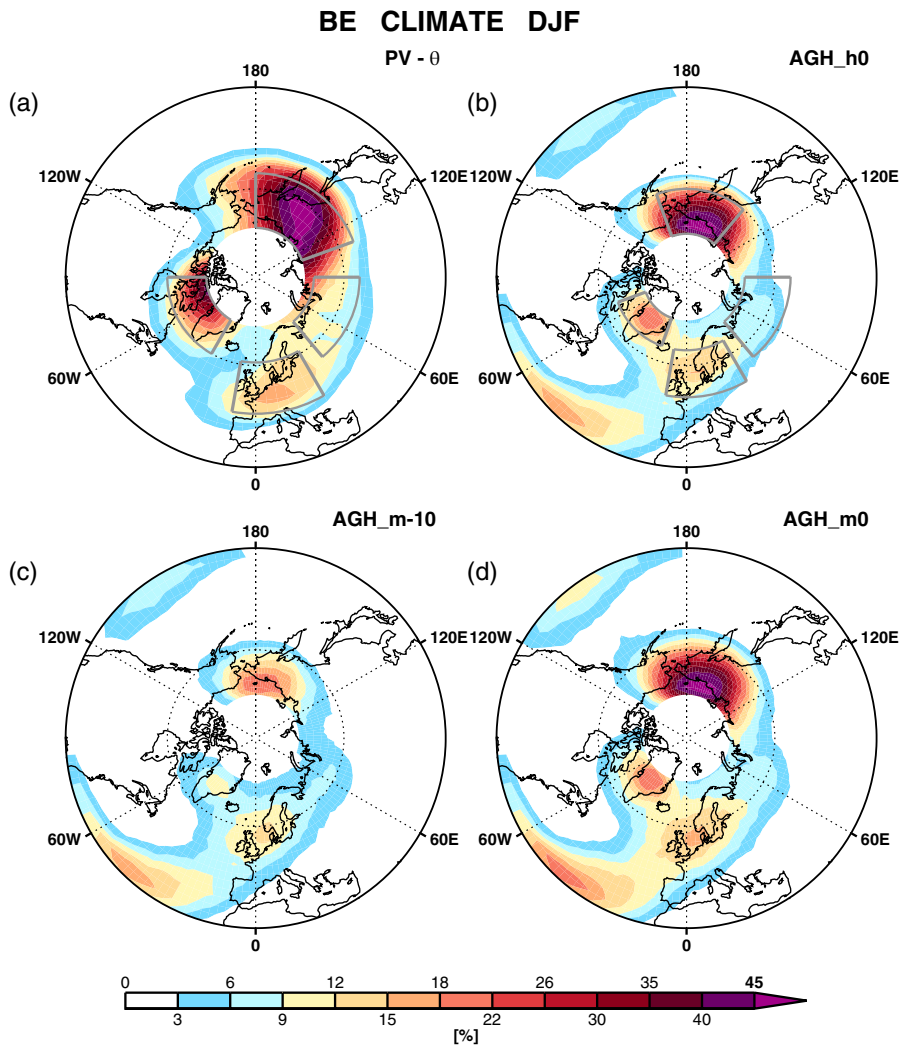


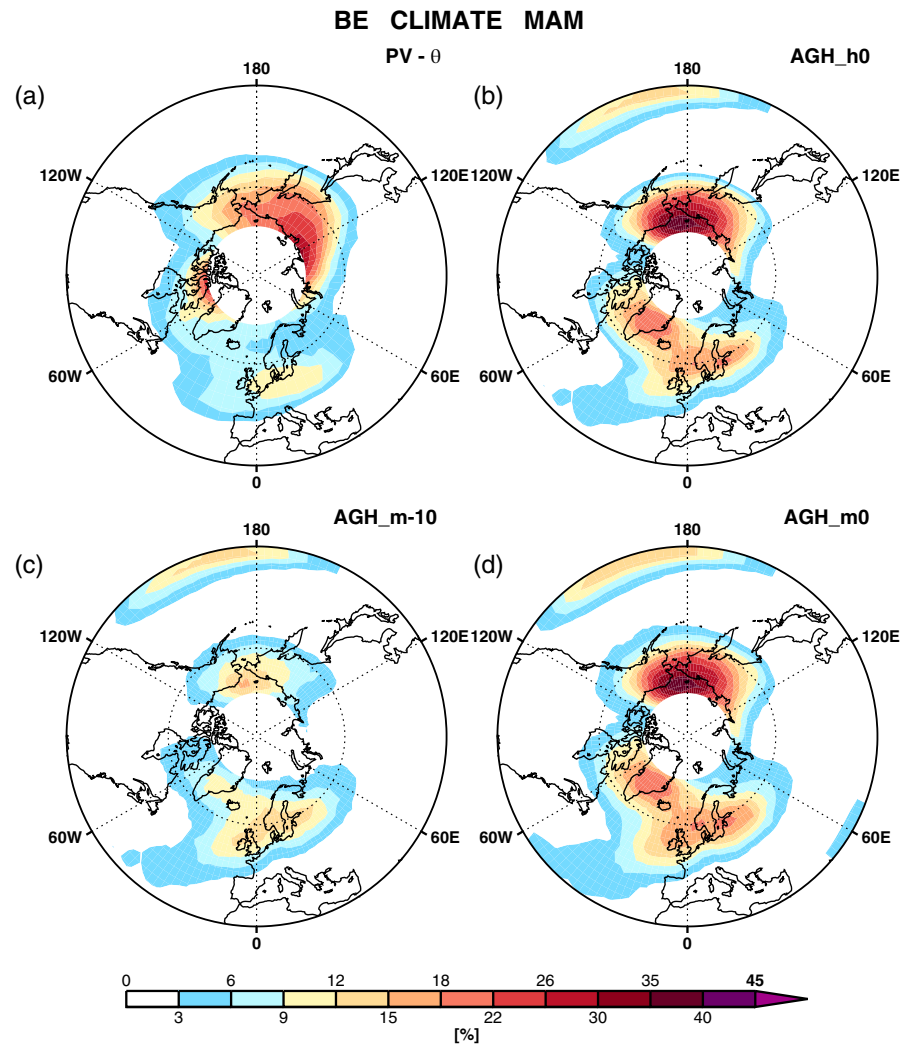
FIGURE 2 Winter (DJF)-mean Blocking Episode (BE) frequencies over the Northern Hemisphere diagnosed by (a) the 2D PV- θ blocking index and (b-d) modified versions of the 2D blocking index introduced by D12. In (c) the value $CT = -10 \text{ m} (\text{°lat})^{-1}$ is assigned throughout the Hemisphere (AGH_m-10) while in (d) the value $CT = 0 \text{ m} (\text{°lat})^{-1}$ is used instead (AGH_m0). In the hybrid case (b) the value $CT = 0 \text{ m} (\text{°lat})^{-1}$ is applied northwards of 60°N while elsewhere the value $CT = -10 \text{ m} (\text{°lat})^{-1}$ is retained (AGH_h0). Box areas in (a, b) delineate the regions over which the BE frequency is area-averaged to calculate the interannual variability of blocking activity over Greenland, Europe, Urals and the Bering Strait (Section 5). The borders of these boxes are different for the two different blocking identification algorithms to capture the slight differences in the salient features of blocking activity over the Northern Hemisphere (see text). For the PV- θ blocking index, the domains are defined as follows: Greenland ($30\text{--}90^\circ\text{W}$, $60\text{--}73^\circ\text{N}$), Europe ($10^\circ\text{W}\text{--}30^\circ\text{E}$, $45\text{--}61^\circ\text{N}$), Ural Mountains region ($40\text{--}90^\circ\text{E}$, $55\text{--}70^\circ\text{N}$) and the Bering Strait region ($110\text{--}180^\circ\text{E}$, $55\text{--}73^\circ\text{N}$). For the modified versions of the AGH algorithm the equivalent domains are defined as follows: Greenland ($20\text{--}70^\circ\text{W}$, $65\text{--}75^\circ\text{N}$), Europe ($10^\circ\text{W}\text{--}30^\circ\text{E}$, $50\text{--}65^\circ\text{N}$), Ural Mountains region ($40\text{--}90^\circ\text{E}$, $55\text{--}70^\circ\text{N}$) and the Bering Strait region ($140^\circ\text{E}\text{--}160^\circ\text{W}$, $60\text{--}75^\circ\text{N}$)

climatology of HLB that converges with that obtained by the PV- θ blocking index (Figure 2a,b). An increase in BE frequency over northern Europe and especially the eastern portion of the Ural sector is evident. The increase in BE activity is striking in the vicinity of the maxima of HLB activity over Greenland and the Bering Strait. Not surprisingly, these are the regions for which the PDFs of westerly flow intensity are shifted towards weaker values further away from the original CT of 8 m s^{-1} (Figure 1d).

The modification of the CT to $0 \text{ m} (\text{°lat})^{-1}$ should be restricted only to latitudes higher than 60°N otherwise some weaker midlatitude blocks will be also included (Figure 2b,d). For latitudes lower than 60°N , the traditional value of $-10 \text{ m} (\text{°lat})^{-1}$ is used. Interestingly, the adoption of $CT = 0 \text{ m} (\text{°lat})^{-1}$ (AGH_m0) also for lower latitudes leads to only a moderate increase by

2–3% in the blocking activity over Europe (Figure 2b,d). This implies that, for midlatitude BEs, the equatorward criterion for the identification of large-scale easterly out-breaks is the most determining factor. The equatorward criterion is satisfied for around 16–17% of the winter days over northern Europe (Figure S6c), while the adoption of $CT = 0 \text{ m} (\text{°lat})^{-1}$ (AGH_m0) or $CT = -10 \text{ m} (\text{°lat})^{-1}$ (AGH_m-10) result in blocking activity over Europe of just above 12% or 15%, respectively (Figure 2b,c). Therefore it is the equatorward criterion which is the primary selector of BE days in the midlatitudes. When this condition is satisfied, the overwhelming majority of the selected blocking highs are already strong enough not only to induce easterlies on their equatorward side, but also have strong enough westerly flow on their poleward side to fulfill the poleward criterion. On the other hand, it is evident from Figure

FIGURE 3 As Figure 2, but for spring (MAM)-mean Blocking Episode (BE) frequency



S6c that over Greenland (Bering Strait) the equatorward criterion is satisfied for around 30–40% (50–60%) of the winter days, while the adoption of $CT = 0 \text{ m } (^{\circ}\text{lat})^{-1}$ (set-up AGH_h0) results in HLB activity over the region that is just above 20% (40%) and much less for the algorithm set-up AGH_m-10 (Figure 2b,c). Thus, in contrast to midlatitudes, for high-latitude BEs, the poleward criterion is the most crucial one because a very strict criterion can severely restrict the identification of persistent easterly outbreaks by the equatorward criterion. Such an ambiguity is not present in methods that detect blocks in regions of easterly flow outbreaks without any additional criteria that can sometimes render the method subjective. The use of a more gradually varying CT with latitude, in which an intermediate value of $-5 \text{ m } (^{\circ}\text{lat})^{-1}$ in the latitude band of $55\text{--}65^{\circ}\text{N}$ is applied, returned only small changes in the winter blocking frequency profiles (compare Figure 2b to Figure S7a for DJF).

Similar convergence in the HLB activity between the two methods is also observed during transitional seasons with the adoption of a $CT = 0 \text{ m } (^{\circ}\text{lat})^{-1}$ for both the

Atlantic and Pacific sectors of the Arctic basin (Figures 3 and 5). However, during boreal summer a slightly different picture emerges. Both the PV- θ and AGH_m-10 algorithms return comparable BE frequency over the Pacific sector, but the maximum over Greenland is much stronger in the diagnosis based on the PV- θ blocking index, as in the winter case (Figures 4a,c). In agreement with previous studies (e.g., figure 2 in Woollings *et al.*, 2018), the AGH_m-10 yields a higher incidence of BEs over Asia and in particular the Ural sector where actually the blocking activity is higher than the winter climatology (Figures 2c and 4c). The modified version of the algorithm (AGH_h0) increases the blocking activity over Greenland to similar levels as those for the PV- θ index, but it may result in excessive blocking detection over Eurasia and the Pacific (Figures 4a,b).

This zonal asymmetry in the dependence of the BE frequency change after the adoption of a less strict CT is due to an east–west asymmetry in the large-scale summer circulation. Unlike boreal winter and transitional seasons, when weak westerlies or easterlies dominate over

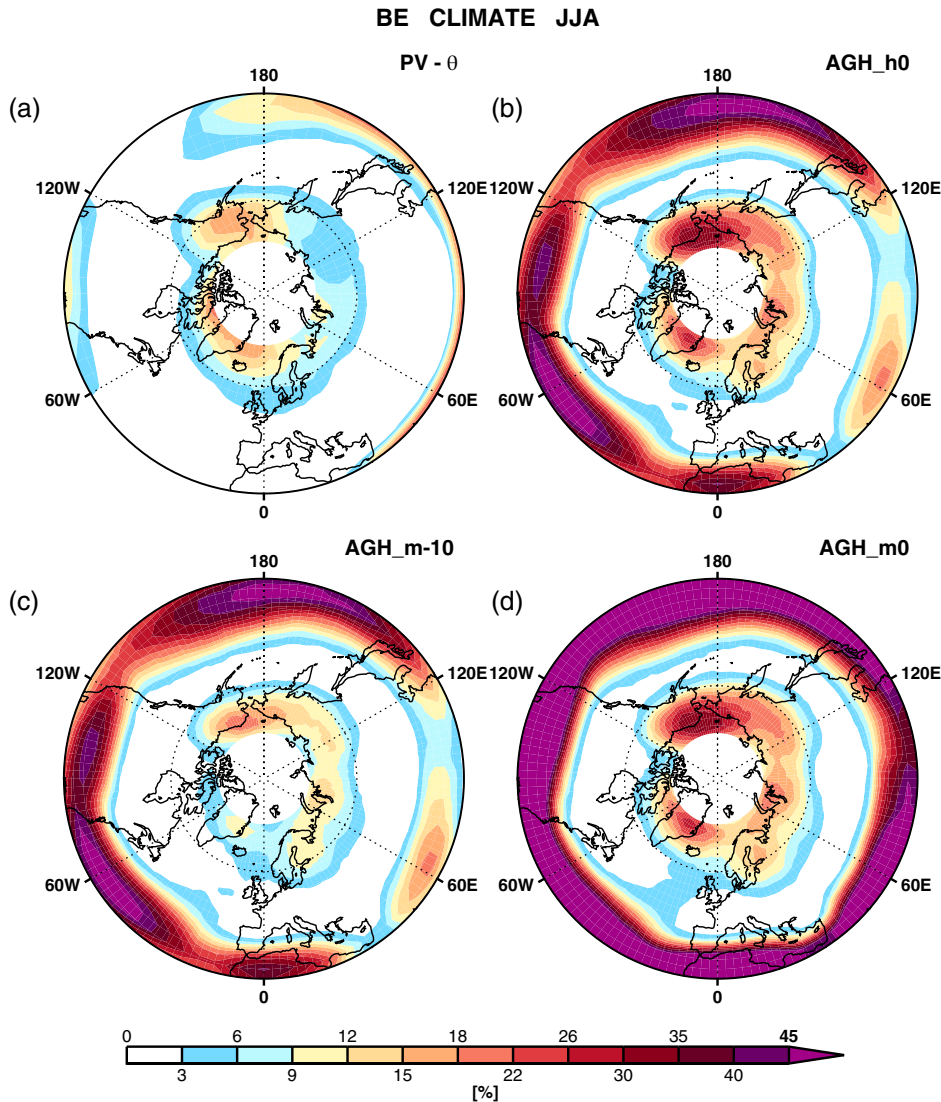


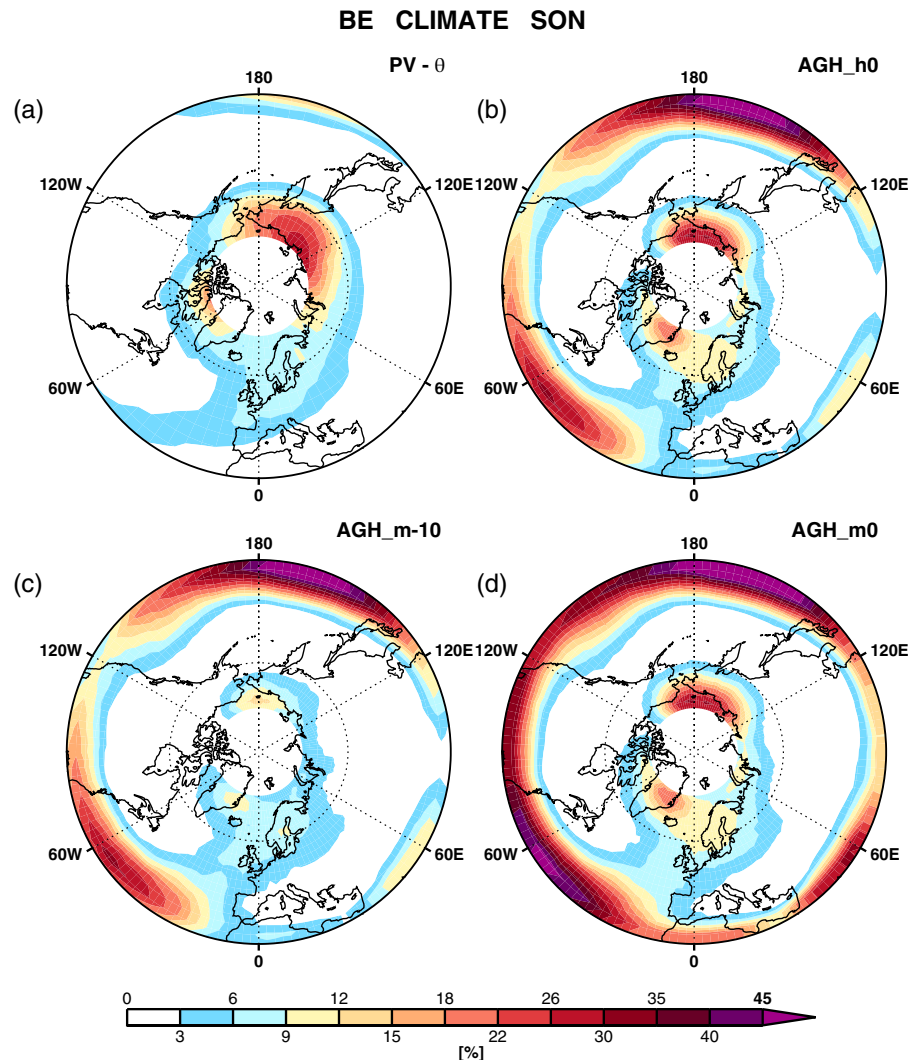
FIGURE 4 As Figure 2, but for summer (JJA)-mean Blocking Episode (BE) frequency

the polar cap without zonal dependence, during summer an east–west split appears; a weak westerly jet dominates along the Siberian and Alaskan coasts. In contrast, the easterly flow over parts of Greenland appears to be actually stronger than in winter (Figure S4). In the transition from winter to summer, an increase (decrease) in the cumulative frequency of summer days that potentially satisfy the poleward criterion is observed to the east (west) of the Urals (Figures 1a and S1a). It could be argued that the adoption of the value $0 \text{ m } (\text{°lat})^{-1}$ for the CT is too loose and allows oversampling of summer HLB over Asia and the Pacific (blue and green curves in Figure S1d) and perhaps a more rigid threshold of $-5 \text{ m } (\text{°lat})^{-1}$ is more appropriate. However, a seasonal dependence in the CT would render the algorithm complex and subjective. In conclusion, for most regions and seasons the adoption of a less strict CT for the poleward criterion allows the convergence of the blocking climatology with other methods. The fact that the influence of the choice of CT on blocking detection

depends not only on latitude and season but also on longitude raises concerns about its subjectivity. Other methods that employ one criterion to identify large-scale and persistent easterlies outbreaks, such as the $PV-\theta$ blocking index or the algorithm employed by Masato *et al.* (2013b), do not suffer from similar ambiguities arising from additional criteria whose efficiency depends on the background flow and its variability.

We further investigate the dependence of the area-averaged BE frequency over the main centres of winter blocking activity on the choice of the CT of the poleward criterion (Figure 6). There is a linear relationship between HLB activity over Greenland and the Bering Strait regions and the value of the threshold. Similar profiles are also obtained for the remaining seasons (not shown). As the CT approaches $0 \text{ m } (\text{°lat})^{-1}$, more days are categorised as BE days and this rate is higher during winter. The lack of a plateau in the curves implies that, provided the equatorward criterion is satisfied, there is

FIGURE 5 As Figure 2, but for autumn (SON)-mean Blocking Episode (BE) frequency



no preferred CT value beyond which a further threshold change would be unnecessary, as most BE are already identified. Therefore, there could be more cases in the BE reservoir to be exploited as the CT reaches $0 \text{ m}(\text{°lat})^{-1}$ or even becomes slightly positive. In the next section we will study in detail the signature of these events to determine whether they are characterised by a typical blocking signature. On the other hand, there is clearly a plateau in the profiles for lower-latitude blocking over Europe and the Urals. The frequency of BEs only slightly increases with an increasing CT and it remains constant beyond $-5 \text{ m}(\text{°lat})^{-1}$. This levelling in the curve again highlights the crucial role of the equatorward criterion in identifying midlatitude blocking, which contrasts the dominant role of the poleward criterion in recognising HLB. The algorithms AGH_m-10 and AGH-h0 yield similar BE activity over Europe and the Urals (green and blue curves in Figure 6) because blocking statistics are affected only over the northern parts of these domains with the threshold modification in high latitudes (box regions in Figure 2a,b).

4 | MORPHOLOGY OF NEWLY IDENTIFIED BLOCKING EPISODES

4.1 | Composite signature of high-latitude blocking

We investigate the morphology of the additional days associated with BE that are identified as the CT gradually changes from -10 to $0 \text{ m}(\text{°lat})^{-1}$. For brevity we focus here on winter HLB activity. Figures 7 and 8 show the composite-mean geopotential height and its anomaly from the mean seasonal cycle for all the new winter BE days identified within a box region over Greenland and the Bering Strait, respectively, as CT gradually changes from (a, b) -10 to $-8 \text{ m}(\text{°lat})^{-1}$, (c, d) -4 to $-2 \text{ m}(\text{°lat})^{-1}$ and (e, f) -2 to $0 \text{ m}(\text{°lat})^{-1}$. Note that the composite signatures for the CT change from -8 to $-6 \text{ m}(\text{°lat})^{-1}$ (not shown) are very similar to those for CT steps -10 to $-8 \text{ m}(\text{°lat})^{-1}$, while the ones for CT changes from -6 to $-4 \text{ m}(\text{°lat})^{-1}$ present anomalies whose amplitudes classify

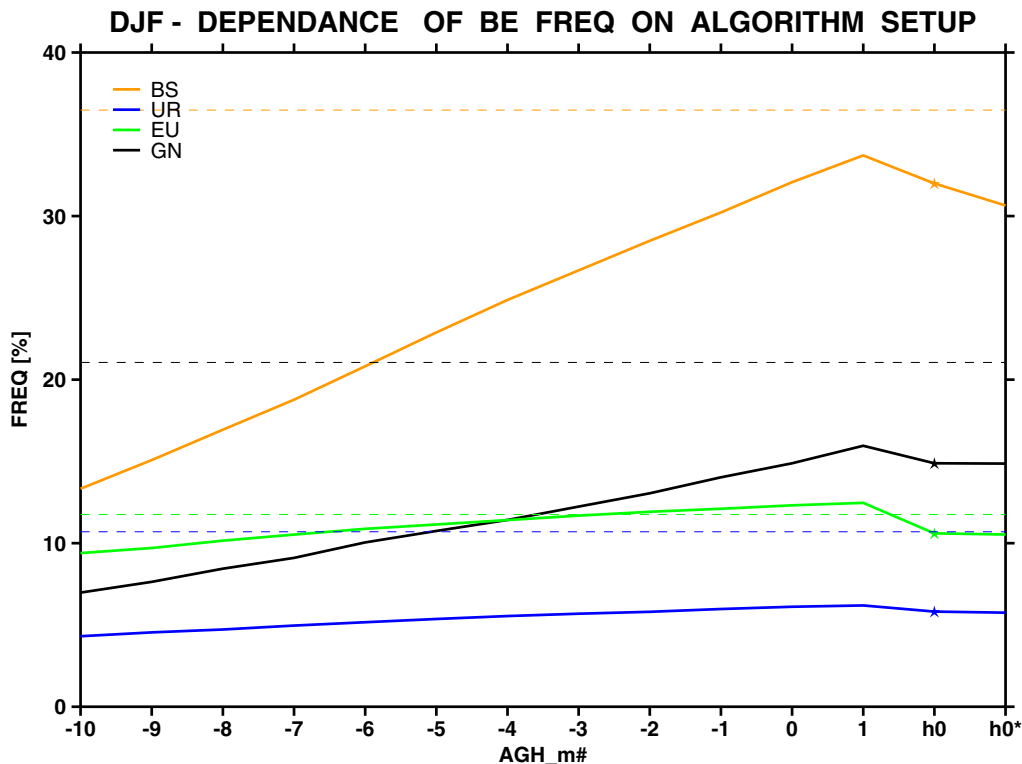


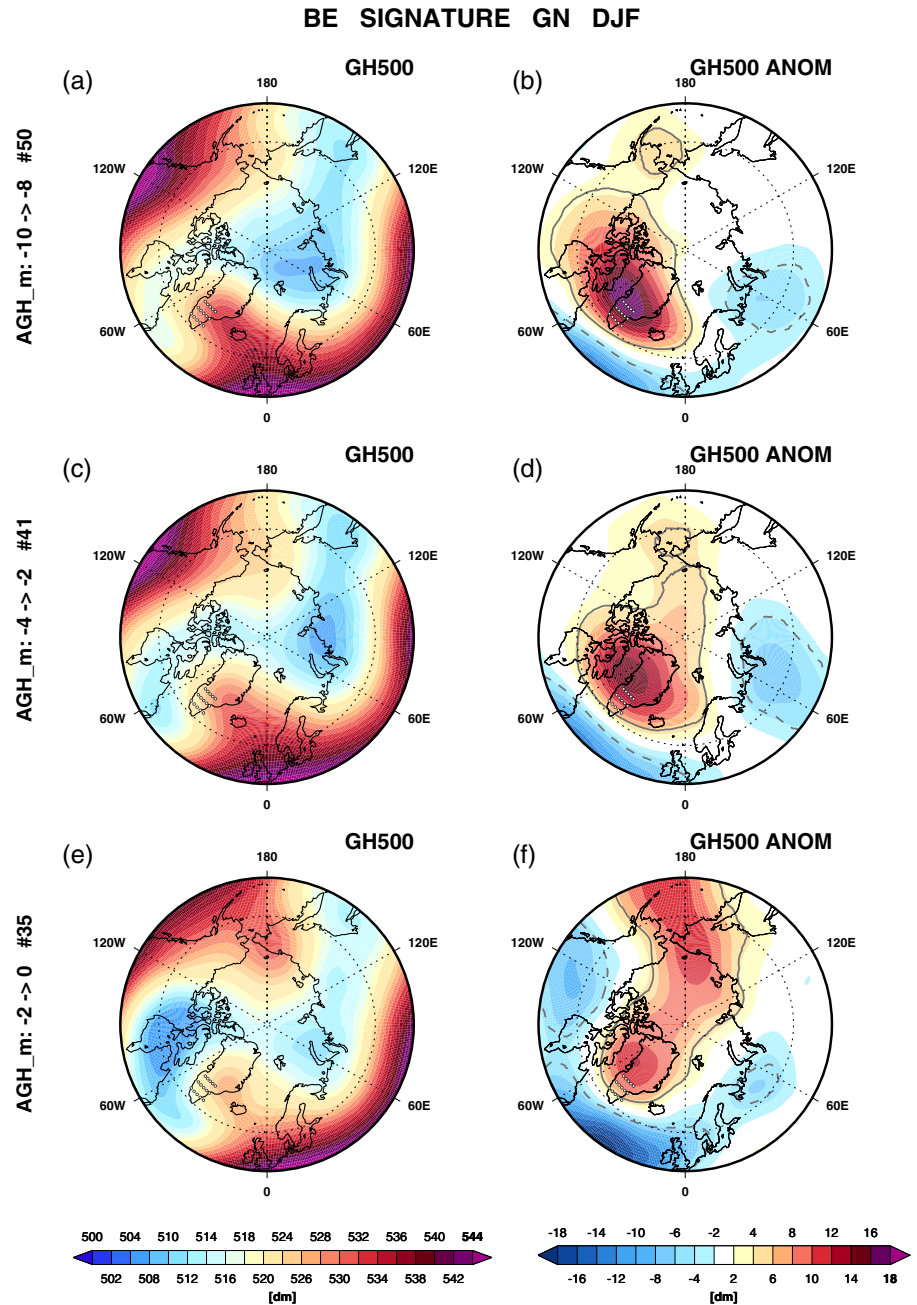
FIGURE 6 Dependence of the regional winter (DJF)-mean Blocking Episode (BE) frequency on the value of the cut-off threshold CT ranging from -10 to $1 \text{ m } (\text{°lat})^{-1}$, labelled on the horizontal axis as a range of set-ups AGH_m-10 to AGH_m1. Additionally, the regional BE activity is shown for algorithm set-ups AGH_h0 and AGH_h0*. CT ranges for the different set-ups are as shown in Table 1. Curves show area-averaged BE frequency over Greenland ($20\text{--}70^\circ\text{W}$, $65\text{--}75^\circ\text{N}$; red line), Europe ($10^\circ\text{W}\text{--}30^\circ\text{E}$, $50\text{--}65^\circ\text{N}$; green line), Ural Mountains region ($40\text{--}90^\circ\text{E}$, $55\text{--}70^\circ\text{N}$; blue line) and the Bering Strait region ($140^\circ\text{E}\text{--}160^\circ\text{W}$, $60\text{--}75^\circ\text{N}$; orange line). These domains are delineated by the boxes in Figure 2b. The value for the algorithm set-up AGH_h0* is marked by a star of the corresponding colour for each region. These values should be compared with the DJF-mean BE frequency diagnosed with the aid of the 2D PV- θ blocking index, which is area-averaged over GN (black dashed line), EU (green dashed line), the Ural Mountains region (blue dashed line) and the Bering Strait (orange dashed line). Note that the box regions for the area averaging for the PV- θ blocking index are slightly different from the ones used in the AGH algorithms and are depicted in Figure 2a

midway through the transition to CT values closer to zero and will also not be shown here. For both regions, the new BE days are characterised by the typical reversal of the meridional height gradient associated with blocking. The blocking ridges are located over Greenland and Far East Asia with troughs to their south. They also have a cyclonic wave breaking signature that is typical for oceanic blocking; they arise from wave breaking (Thorncroft *et al.*, 1993; Peters and Waugh, 1996; Gabriel and Peters, 2008) that leads to poleward (equatorward) extrusions of warm (cold) air masses with a cyclonic direction of wave breaking.

Cyclonic wave breaking is typical on the poleward side of the midlatitude jet where a positive horizontal wind shear prevails (Tyrlis and Hoskins, 2008b; Masato *et al.*, 2012; 2013a). Given the pronounced southwest-northeast tilt in the North Atlantic jet, cyclonic wave breaking dominates over the northwestern parts of the basin. Consistent with Figure 6, a large number of winter days associated with BE are added (especially over the Bering

Strait) even when the CT becomes -2 or $0 \text{ m } (\text{°lat})^{-1}$ (Figures 7c,e and 8c,e). These BE days are still characterised by the presence of a dipole of statistically significant height anomalies and a typical reversal of geopotential height akin to cyclonic wave breaking similarly to the events identified for more strict values of the CT (Figures 7a and 8a). Thus, they cannot be easily discarded as cases of, for example, cut-off lows. It is worth noting that all BEs identified by the algorithm fulfill all the necessary criteria of temporal persistence and extensive spatial coverage; cases of transient cut-off lows are excluded by design. As the threshold approaches to $0 \text{ m } (\text{°lat})^{-1}$, the anticyclonic anomaly over Far East Asia and especially Greenland weakens significantly and thus the reversal of the meridional gradient is mainly sustained due to the strong trough lying to the south of the anticyclone (Figures 7b,d,f and 8b,d,f). Masato *et al.* (2012; 2013a) categorised blocks as warm or cold depending on whether the poleward warm air extrusion or equatorward

FIGURE 7 (a, c, e) Composite mean signature of geopotential height (dm) at 500 hPa and (b, d, f) its anomaly from the mean seasonal cycle for the additional winter (DJF) days featuring BEs that are identified over Greenland (GN; 40–50 °W, 62.5–67.5 °N) as the CT changes (a, b) from -10 to -8 $\text{m}(\text{°lat})^{-1}$, (c, d) from -4 to -2 $\text{m}(\text{°lat})^{-1}$ and (e, f) -2 to 0 $\text{m}(\text{°lat})^{-1}$. In each algorithm set-up the value of the CT is assigned throughout the Northern Hemisphere (e.g., AGH_m-2 for $\text{CT} = -2$ $\text{m}(\text{°lat})^{-1}$). The mean signature and its anomaly are calculated for each grid-point marked by a dot and then averaged over the whole box region. The number shown in each row of panels corresponds to that of new days featuring BE over Greenland that are identified after the change of CT; it is the arithmetic mean (rounded to the nearest integer) of all the new days identified for all grid-points over Greenland. The mean daily seasonal cycle was subtracted from the daily mean timeseries to construct daily mean anomalies of geopotential height at 500 hPa. The statistical significance of the anomalies shown in (b, d, f) is assessed with the aid of a Monte Carlo robustness test (Section 2). In the case that the observed composite mean anomaly of the new BE days at a given grid-point ranks in the upper (lower) 2.5% of the synthetic distribution of samples generated by the Monte Carlo process, then the specific grid-point is enclosed by the solid (dashed) line and the anomaly is deemed as statistically significant at the 95% confidence level



cold air extrusion in the upper troposphere is the dominant feature. A reasonable assumption can be made that a strong (weak) poleward warm air extrusion is associated with a strong (weak) ridge and a strong (weak) equatorward cold air extrusion is associated with a strong (weak) trough. Thus, it can be said that, as the CT becomes less strict, there could be more (less) newly recognised BE days that are associated mainly with cold- (warm-) cyclonic blocking over both the Atlantic and Pacific sectors.

Over Europe and especially over the Urals, a number of new cases is added when the CT drops below -4 $\text{m}(\text{°lat})^{-1}$ to -2 or 0 $\text{m}(\text{°lat})^{-1}$ (Figures 9 and S8). Consistent with the slopes of the curves shown in Figure 6, the increase in number of days is substantially smaller

than in the case of Greenland or the Bering Strait. Most BE days are already captured even by the original cut-off threshold of -10 $\text{m}(\text{°lat})^{-1}$ and a relatively small number of cases is added when the CT is modified. European BEs resemble dipole blocks that are the result of anticyclonic wave breaking taking place at the exit of the North Atlantic storm track. Anticyclonic wave breaking prevails at the exit of the North Atlantic jet where the background flow is characterised by an anticyclonic horizontal wind shear (Tyrlis and Hoskins, 2008b). Ural BEs have the composite signature of Rex-type blocks; the Ural sector lies between the maxima of blocking activity over Europe and Far East Asia. The ‘hybrid’ composite signature could be the result of amalgamation of cases of

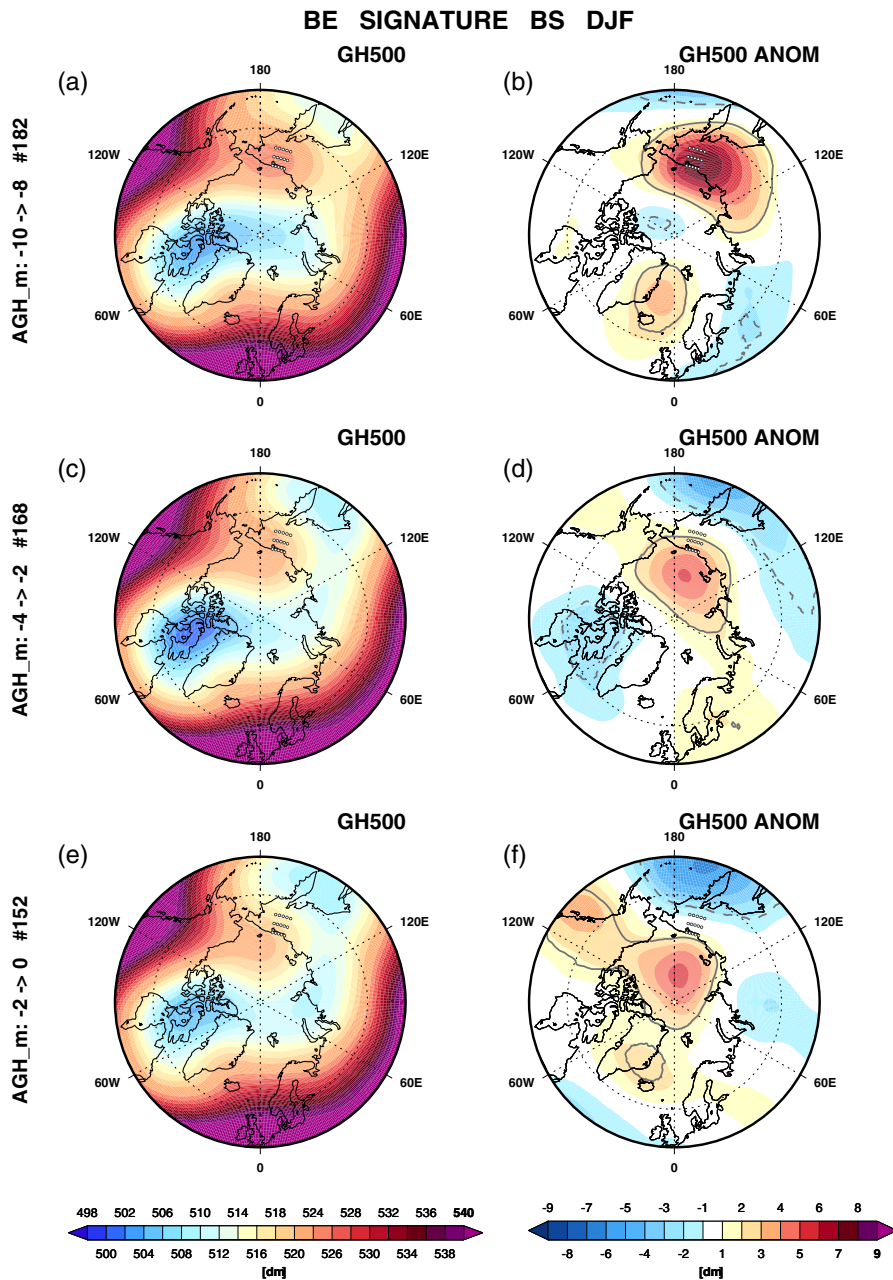


FIGURE 8 As Figure 7, but for the additional winter (DJF) days featuring Blocking Episodes (BEs) that are identified near the Bering Strait (BS; 160–170°E, 65–70°N)

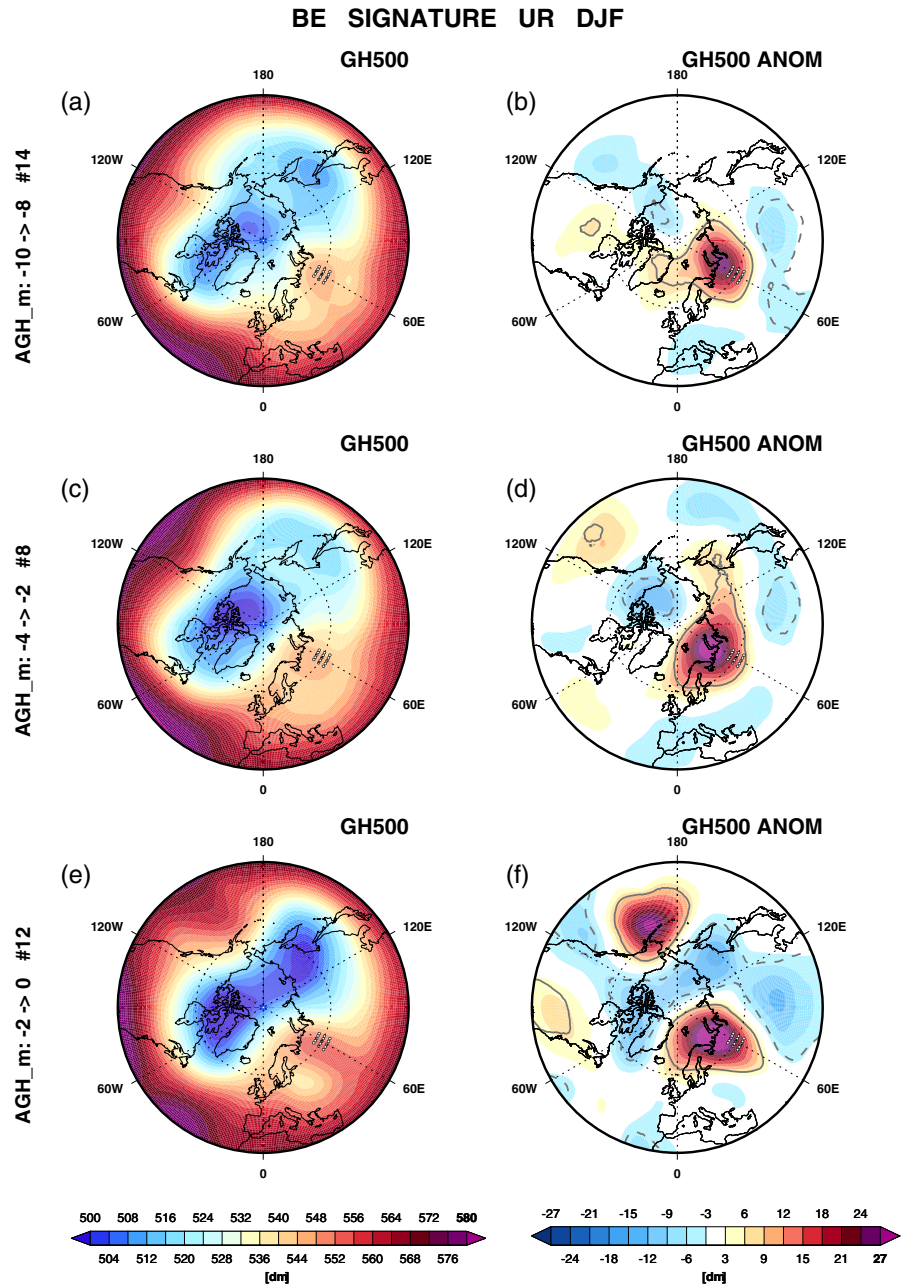
anticyclonic (cyclonic) wave breaking over the western (eastern) parts of the Ural sector (Masato *et al.*, 2012). Westward retrogression of blocks initially developed over the Pacific towards the Ural sector has also been reported (e.g., Takaya and Nakamura, 2005). The anomalous blocking signature over Europe and the Urals appears to be stronger for higher thresholds (Figures 9b,d,f and S8b,d,f). However, unlike in the case of HLB, a fair comparison cannot be made because the number of additional cases is small and decreasing even further for nearly zero values of the CT. Thus, the composite could be dominated by a few days of very strong blocking signature due to its small sample, though it is worth noting that all anomalies were found to be statistically robust. Finally, although that the

number of sample size in the composite means shown in Figures 7–9 and Figure S8 is not always comparable, consistent with previous studies (e.g., Woollings *et al.*, 2008; Davini *et al.*, 2012), the anomalous signature of HLBs is weaker than midlatitude blocking over Europe and central Asia (note the different scale in the corresponding colour bar).

4.2 | Greenland blocking

A detailed investigation of the changes in the temporal distribution of HLB at a representative location over Greenland (50°W, 67.5°N) as the CT changes from –10 to

FIGURE 9 As Figure 7, but for the additional winter (DJF) days featuring Blocking Episodes (BEs) that are identified over the Urals (UR; 55–65°E, 57.5–62.5°N)



$0 \text{ m} (\text{°lat})^{-1}$ suggests that there is not only a prolongation of the duration of BEs with the earlier onset or later lysis of a BE, but fresh BEs emerge as the CT becomes less strict (Figure 10). A large number of added BE days over Greenland for all seasons has been randomly selected, belonging to both newly added BEs and those already existing but prolonged (marked by blue triangles in Figure 10). Figures 11,12, S9 and S10 illustrate the daily mean geopotential height (colour shades) and its anomaly from the mean seasonal cycle (contours) for newly detected Greenland BE days for a selection of CT modifications both in the lower and higher band of the threshold range. In each case, three winter BE days are included and one for each of the remaining seasons. We cannot identify a case

that lacks the typical blocking signature that can justify their rejection as BE. Most significantly, a blocking ridge is always present over Greenland, even when the CT is modified to include days featuring only a weak poleward westerly flow (Figures 12, S10). Similarly to the composite means illustrated in Figure 7, for BE occurring in winter and transitional seasons, as the CT becomes higher than $-2 \text{ m} (\text{°lat})^{-1}$, the anticyclone weakens and the trough to its south becomes the dominant feature, which is typical for cold-cyclonic wave breaking leading to blocking over the western Atlantic (Masato *et al.*, 2012; 2013a). Across the whole range of CT values, summer BEs are characterised by the presence of a strong blocking high over Greenland and cyclonic activity over the North Atlantic

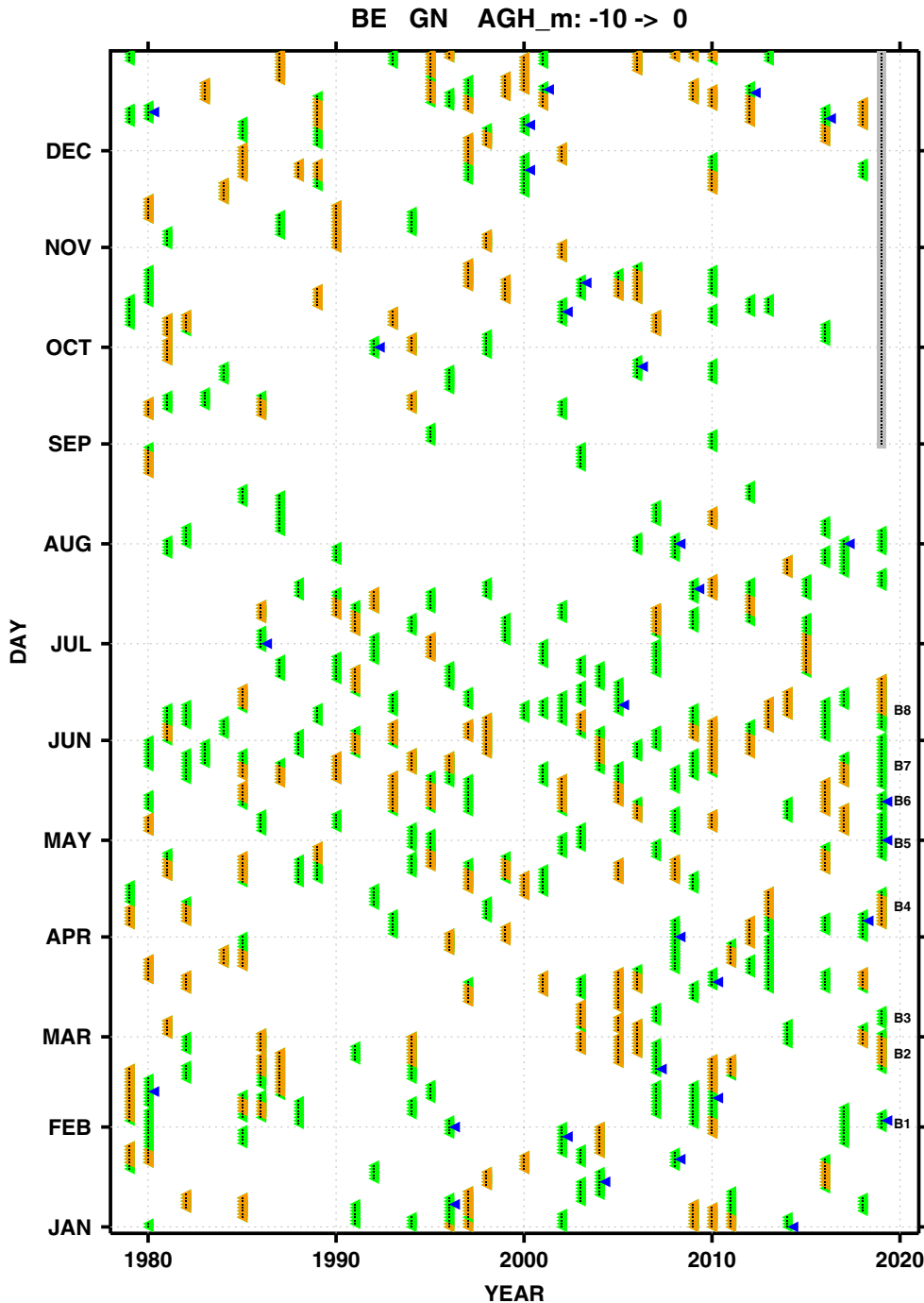


FIGURE 10 Scatter plot illustrating the occurrence of Blocking Episode (BE) days identified over Greenland (GN; 50°W, 67.5°N) throughout the ERA-Interim period. BE days identified with the use of the algorithm setup AGH_m-10 are marked by orange left-pointing triangles. Additional BE days that are identified over Greenland as the CT changes from -10 to $0 \text{ m } (^{\circ}\text{lat})^{-1}$ (change of algorithm set-up AGH_m-10 to AGH_m0, which is the same as AGH_h0 for high latitudes) are marked by green left-pointing triangles. These days correspond to the new days added after the modification of the cut-off threshold. All identified BE days over Greenland are marked by black dots lying at the centre of triangles. Blue triangles point to the selected BE days for which the daily-mean fields are shown in Figures 11,12, S9 and S10. The eight BEs identified over Greenland during the first half of 2019 are marked by B1–B8 (Section 4.3)

that sustains the easterly flow over the northern parts of the oceanic basin.

4.3 | The extreme event of Greenland ice sheet melting in summer 2019 and its link to blocking

In June 2019 a record breaking episode (marked B8 in Figure 10) of very early Greenland ice sheet melting took place (e.g., Witze, 2019). The ice melting peaked on 12 June

(Figure S11) following a warm spring when anticyclonic conditions prevailed over Greenland. Enhanced melting of Greenland ice and sea-ice surrounding the peninsula have been often linked to Greenland blocking (Overland *et al.*, 2012; McLeod and Mote, 2016; Ballinger *et al.*, 2018; Wang *et al.*, 2019). This is potentially linked to the enhanced poleward intrusion of warm and moist air towards Greenland induced by the blocking anticyclone, leading to the local intensification of downward infrared radiation and increased short-wave radiation in clear-sky regions (Woods *et al.*, 2013; Woods and Caballero, 2013;

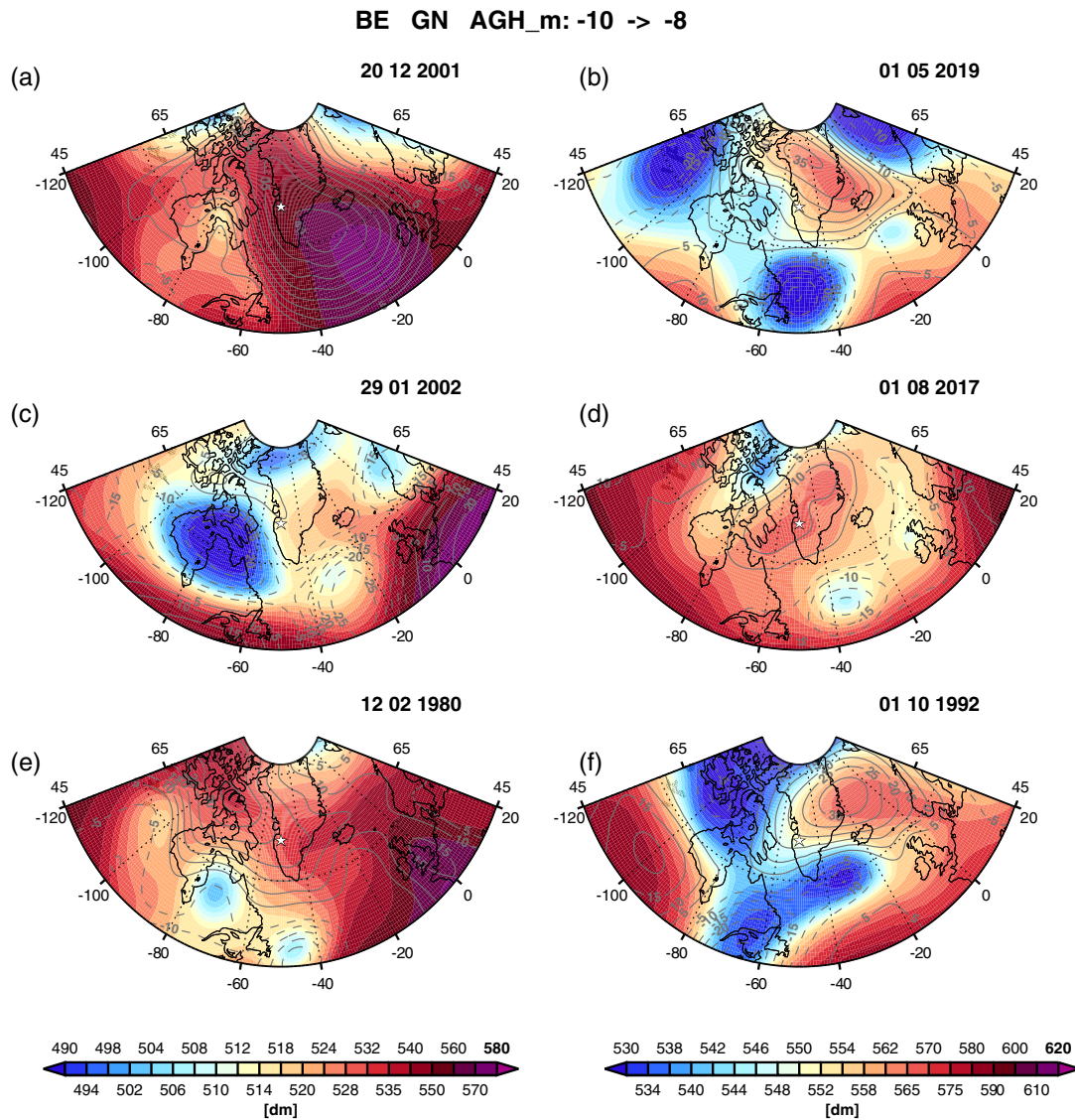


FIGURE 11 Daily-mean geopotential height (filled contours, in dm) and anomaly from the mean seasonal cycle (contours, in dm) at 500 hPa for a selection of new days associated with Blocking Episodes (BEs) over a grid-point in Greenland (GN; 50°W, 67.5°N marked by star) after the change of the CT from -10 to -8 $(^{\circ}\text{lat})^{-1}$ (change of algorithm from set-up AGH_m-10 to AGH_m-8). These days are marked by blue triangles in Figure 10. Note that the mean daily seasonal cycle was subtracted from the daily mean timeseries to construct timeseries of daily mean anomalies of geopotential height at 500 hPa

Lee *et al.*, 2017; Hermann *et al.*, 2020). Arctic anticyclones, which often result from extratropical cyclones injecting extratropical air masses with low potential vorticity into the Arctic upper troposphere, are of key importance for influencing the variability of the overall summertime Arctic sea-ice melting (Papritz and Wernli, 2018).

Blocking activity diagnosed with the aid of the PV- θ blocking index over Greenland in spring 2019 was approximately 20% higher than the climatological mean of around 10% (Figure 13a,b). Abundant springtime blocking activity, and induced warm advection from northeastern Canada towards Greenland, combined with clear skies, must have contributed to the heating of the snow pack over

Greenland and caused its melting in early June. Strikingly, if the original AGH algorithm is employed, only a very weak positive BE frequency anomaly can be recognised (Figure 13e,f). Indeed, only episode B2 in late February, B4 in early April 2019 and the strong episode (B8) in early June that caused the excessive ice melting were identified by the AGH algorithm (Figure 10). The number of identified BEs in April and May 2019 increases substantially when the CT is modified to 0 $(^{\circ}\text{lat})^{-1}$ (marked B1–B8 in Figure 10) resulting in a seasonal BE frequency anomaly over Greenland that is comparable to the one obtained by the PV- θ blocking index (Figure 13a–d). Evidently, a more appropriate cut-off threshold is crucial for the adequate

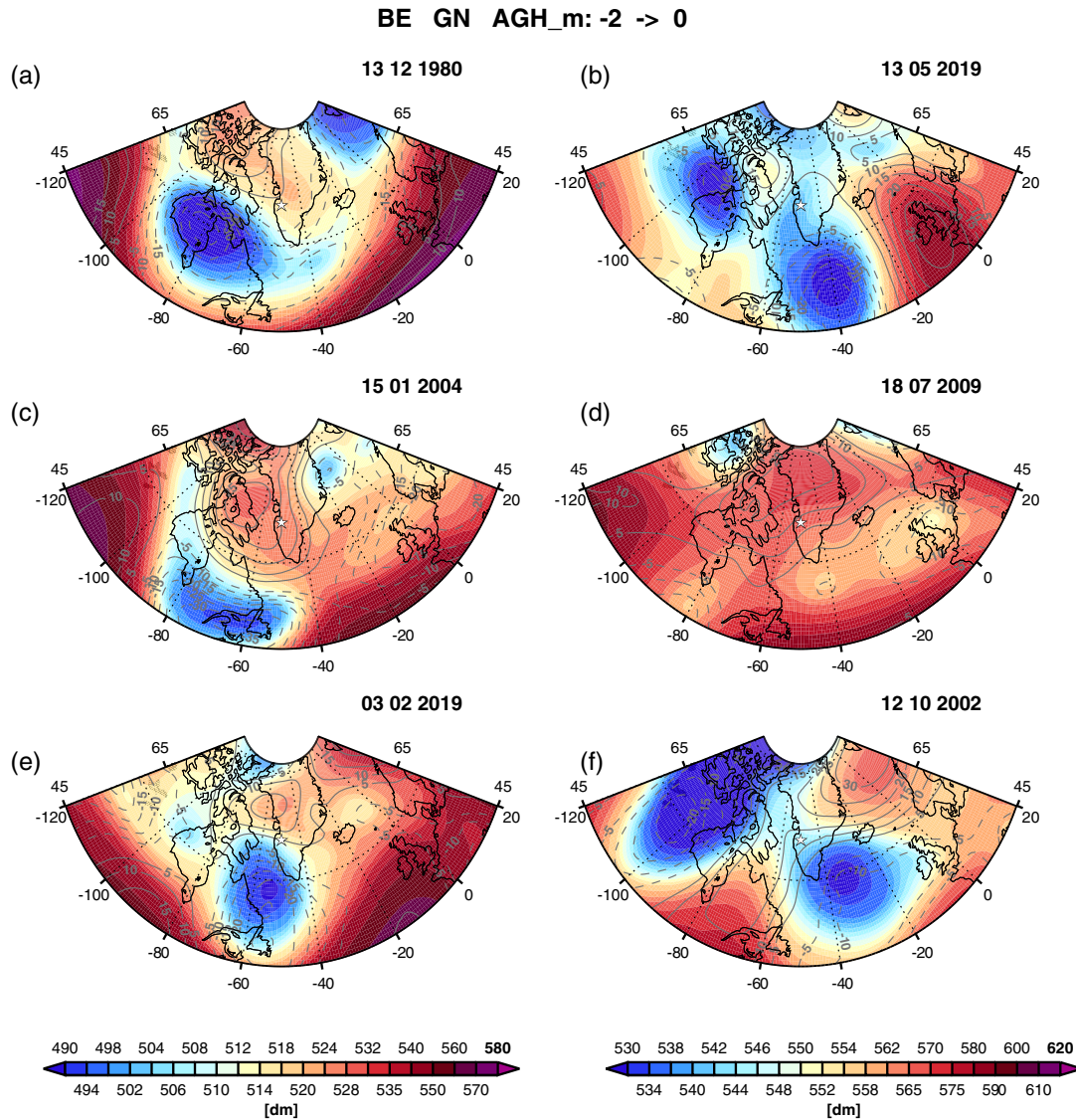


FIGURE 12 As Figure 13, but for a selection of new days associated with Blocking Episode (BE) over the grid-point in Greenland after the change of the CT from -2 to $0 \text{ m} (\text{°lat})^{-1}$ (change of algorithm set-up from AGH_m-2 to AGH_m0)

sampling of HLB that enables a thorough understanding of the dynamics causing it as well as its impacts.

5 | INTERANNUAL VARIABILITY AND TRENDS

The winter-mean blocking frequency over the four key regions of Greenland, Bering Strait, Europe and the Urals diagnosed with the modified AGH_h0 algorithm is higher than that obtained with the original AGH_m-10 method for all winters (Figure 14). The increase is lower, as expected, over the Urals and especially Europe, because the CT is only modified over a portion of these domains. The convergence in the blocking activity profiles between

the PV- θ and AGH_h0 indices is higher for the Bering Strait whereas over Greenland it is closer during winters of abundant blocking. Interestingly, over Europe there is an agreement in the profiles obtained by the PV- θ blocking index and both AGH_m-10 and AGH_h0 algorithms (Figure 14c). Over the Ural sector, the PV- θ blocking index tends to detect more blocking than the AGH_h0 algorithm (orange and grey lines in Figure 14d). The winter climatology of BE frequency diagnosed with the former method presents a maximum of blocking activity in the vicinity of the Bering Strait that is detected at a more western location and expanding towards the Ural region compared to the one obtained by the AGH_h0 algorithm (Figure 2a,b). Investigation of the evolution of the record-breaking Ural blocking activity in autumn 2016 by Tyrlis *et al.* (2019)

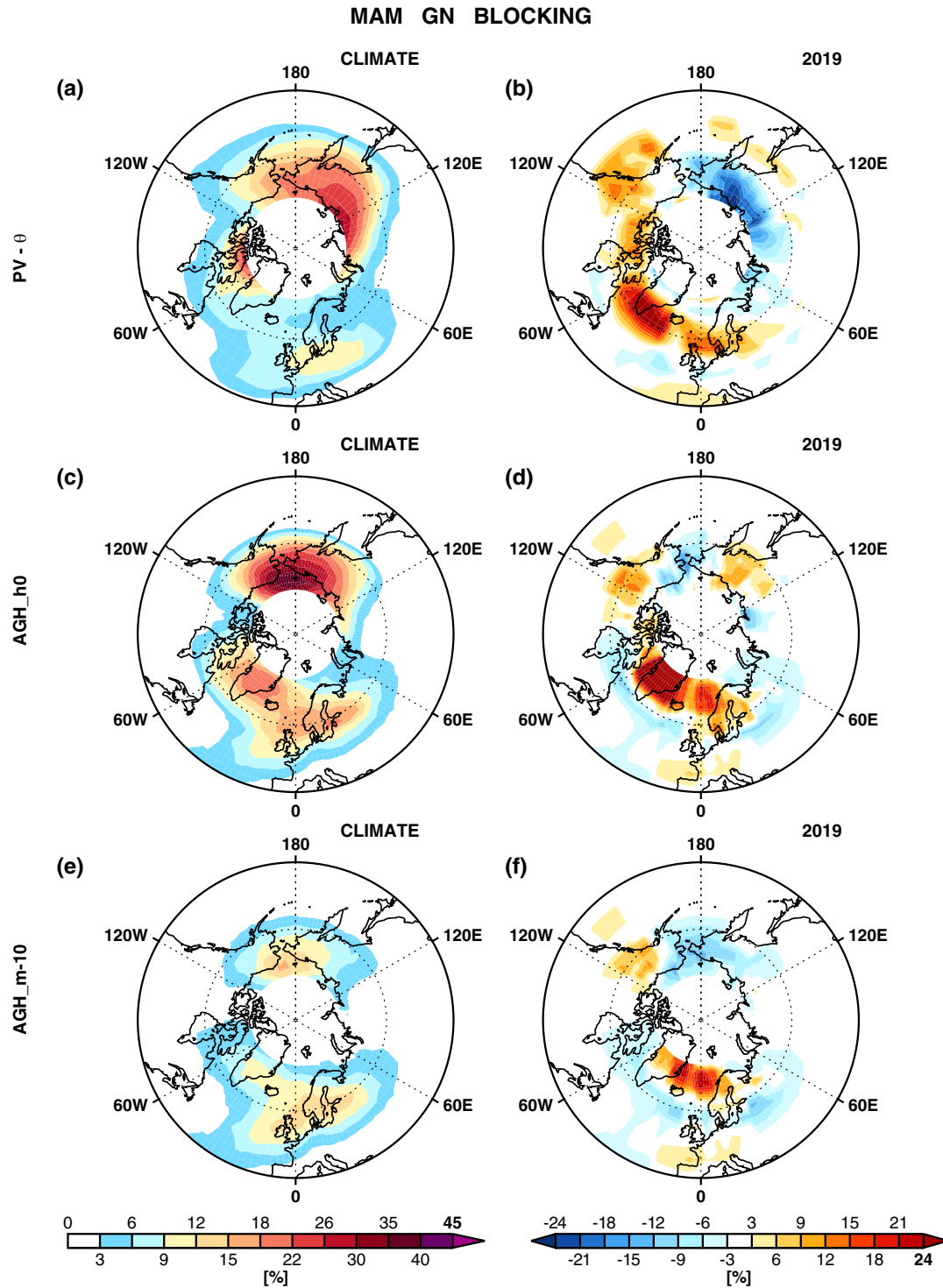


FIGURE 13 Spring (MAM)-mean (a, c, e) Blocking Episode (BE) frequency and (b, d, f) anomalous BE occurrence during spring 2019. The analysis is based on the identification of BEs with the aid of the (a, b) 2D $PV-\theta$ blocking index and (c–f) various modified versions of the AGH algorithm employed by D12, with CT values assigned as in Table 1.

revealed that the $PV-\theta$ blocking index is more sensitive in identifying blocking over the region than blocking detection methods based on various versions of the algorithms employed by TM90, Scherrer *et al.* (2006) and D12. Thus, the understanding of the link between Ural blocking and

Arctic Amplification is facilitated by the more accurate identification of blocking over the region.

Similarly, over the other hot-spot of HLB activity over Greenland, the maximum is again detected over a slightly more southern and western location by the $PV-\theta$ blocking

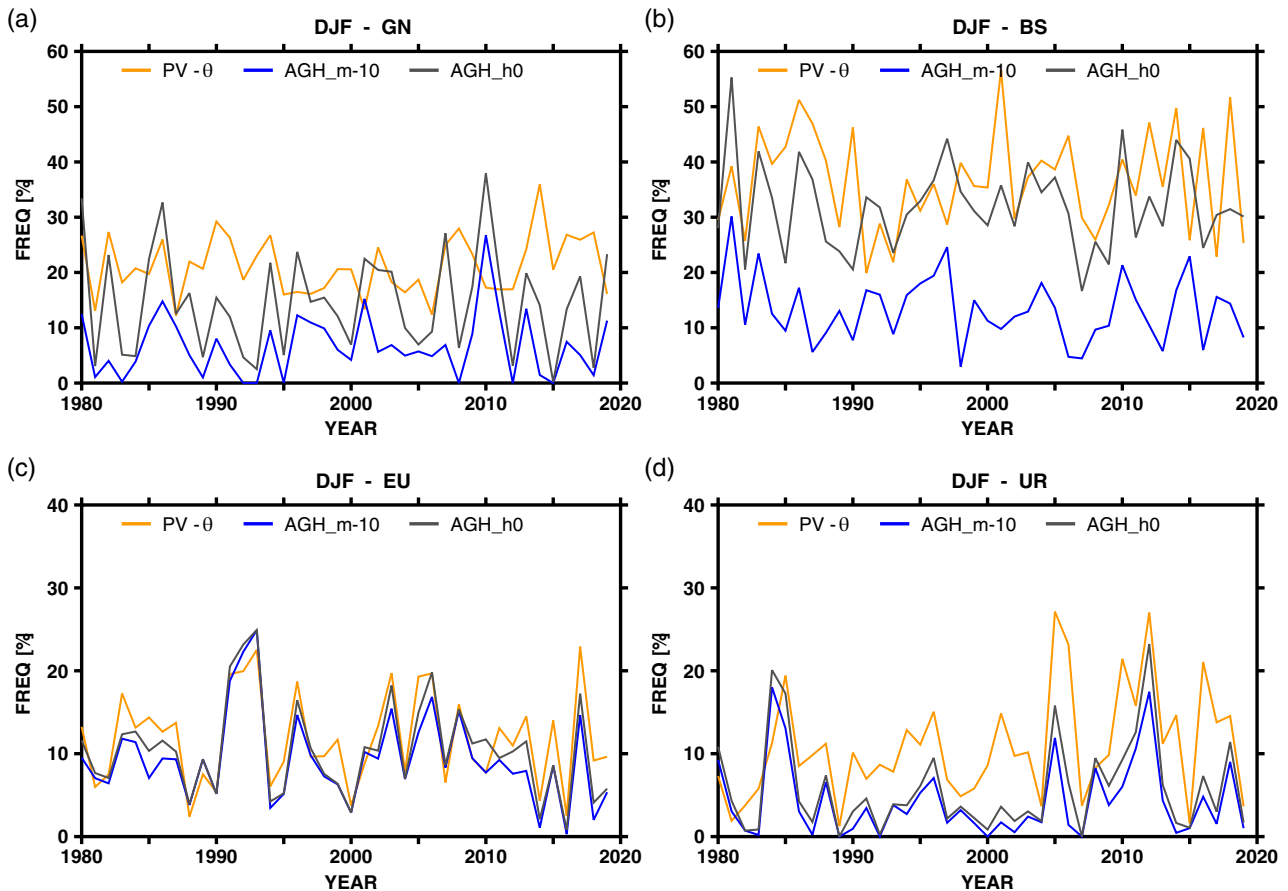


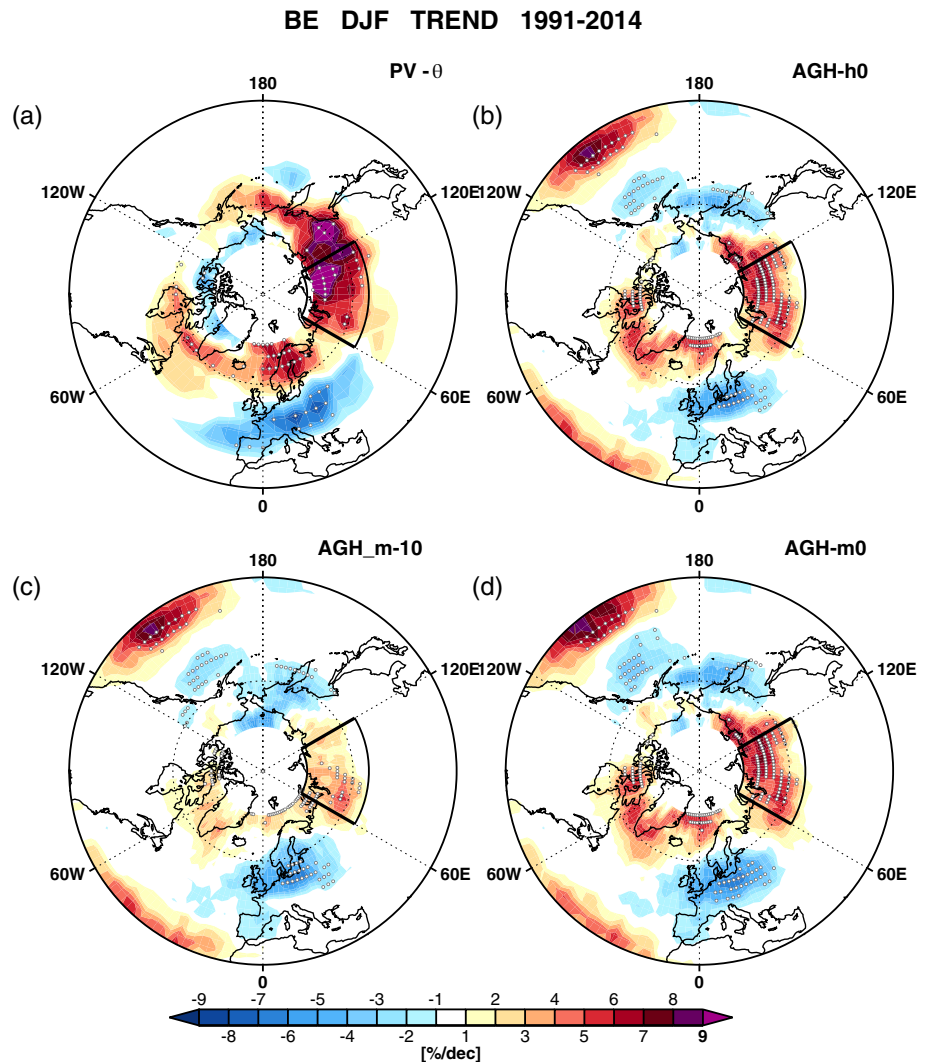
FIGURE 14 Interannual evolution of regional DJF-mean BE frequency area-averaged over (a) GN, (b) BS, (c) EU and (d) UR. Blocking is diagnosed with the aid of the 2D PV- θ blocking index (orange), as well as AGH algorithm set-ups AGH_m-10 (blue) and AGH_h0 (grey), with CT values assigned as in Table 1. Note that the box regions for the area averaging for the PV- θ blocking index are slightly different from the ones used in the AGH algorithms; both are depicted in Figure 2a,b. Each yearly value corresponds to the percentage of winter days featuring BE occurrence during the continuous December–February and labelled by the year of corresponding January. Thus, the BE activity for DJF 2009–2010 is shown as for year 2010. The first element of the timeseries refers to DJF 1979–1980 and the last to DJF 2018–2019

index (Figure 2a,b). Therefore we obtained regional averages of BE frequency over Greenland and the Bering Strait by averaging BE over box domains that are slightly different for the two blocking methods. Such a discrepancy is not surprising given the differences in the two methods. By investigating many cases of winter blocking over the western North Atlantic (e.g., in December 2009, shown in Figure S12), the PV- θ blocking index appears to systematically identify blocking at different locations compared to the AGH_m-10 and AGH_h0 algorithms. Not only does it identify blocking in areas of easterlies, which lie southward of the blocking ridges, but also it tends to enhance blocking recognition on the western flanks of the Greenland ridge. Very low θ values at the tropopause level are common during winter over Canada and even a weak northward intrusion of high- θ air masses can result in reversals of the meridional gradient of θ on the dynamical tropopause. This evolution must be very common over the region where cyclonic wave breaking is very frequent

(Section 4.1) and explains the tendency of the PV- θ blocking index to yield high blocking activity over Canada.

For any given winter, the planetary-scale circulation may be varying in the upper- and mid-troposphere, favouring different locations of preferred blocking which can be different from the box regions shown in Figure 2a,b. A characteristic example is the winter 2009–2010 when blocking was widespread over the European and North Atlantic sectors (Sprenger *et al.*, 2017). Both AGH_m-10 and AGH_h0 algorithms yield prominent maxima in blocking activity; such a maximum is not present in the profiles produced with the PV- θ blocking index (grey and orange lines in Figure 14a). However, the PV- θ blocking index also identifies abundant blocking activity for winter 2009–2010 but at much lower latitudes than the AGH_m-10 and AGH_h0 algorithms (Figure S13) over a region that lies outside the domain used to define the respective timeseries. This accounts for the partial mismatch between the two methods in the peaks of blocking

FIGURE 15 Linear trends of winter (DJF)-mean Blocking Episode frequency (in % per decade) over the Northern Hemisphere during the period 1991–2014. The analysis is based on the identification of BEs with the aid of the (a) 2D PV- θ blocking index and (b-d) various modified versions of the AGH algorithm employed by D12, with CT values assigned as in Table 1. White dots marks grid-points where the trends are statistically significant at the 95% level. The statistical significance of linear trends is evaluated with a two-sided t -test. Note that the resolution of the grid for the PV- θ blocking index is 5° longitude by 4° latitude while for the variants of the AGH algorithm is 2.5° longitude by 2.5° latitude. The box delineates a region over central Siberia (60–120°E, 55–75°N)



activity over Greenland for some winters (Figure 14a). It appears that there is higher year-on-year variability in the location of blocking activity produced by the PV- θ blocking index. This index identifies blocking at the tropopause level, where the planetary-scale circulation changes from year to year are starker than those in the mid-troposphere where the AGH_h0 algorithms identifies blocking. Therefore caution is advised in the choice of the domain for studying HLB when different blocking identification methods are compared.

Tyrlis *et al.* (2020) identified a statistically significant upward trend of winter-mean BE frequency over the Urals during the period 1991–2014. Indeed more frequent blocking activity was observed over the Ural sector after 2000, whereas after 2015 blocking activity over Siberia returned to lower levels (Figure 14d). The increasing Ural blocking activity during the period 1991–2014 was found to be key for inducing the observed cooling over central Asia (Tyrlis *et al.*, 2020). The upward trend in winter blocking

activity during 1991–2014 actually extends over the whole of Eurasia for latitudes higher than 60°N for winter time-series obtained by the PV- θ blocking index (Figure 15a). Specifically, the trend for BE frequency area-averaged over high-latitude central Siberia (60–120°E, 55–75°N) is 6.4% per decade and is statistically significant at the 95% confidence level. Such a statistically robust trend is hardly distinguishable (mainly over the Urals) when the traditional blocking identification algorithm AGH_m-10 is employed (Figures 15c). Interestingly, a higher positive trend can be identified over Eurasia after the adoption of the modified AGH algorithm (Figures 15b,c). The trend of regional BE activity over the aforementioned domain almost doubles from 2.2% per decade to 3.9% per decade (both statistically significant) with the change from algorithm set-up AGH_m-10 to AGH_h0. Thus, pattern and strength of trends of HLB identified by both the two methods converge when a more fitting CT is adopted in the method employed by D12. Note that the upward trend

in blocking activity over central Siberia diminishes and is not statistically significant at the 95% level when data for the entire ERA-Interim period is analysed irrespective of the blocking identification method employed, but certainly is more distinguishable in the case that blocking is identified by the PV- θ and AGH_h0 (Figure S14). For trends obtained by the PV- θ blocking index, an upward trend of 2% per decade was found over central Siberia (black domain in Figure S14a) but it is statistically significant at the 90% confidence level. Our results are consistent with Barnes *et al.* (2014) who found no clear hemispheric increase in winter blocking events over the recent decades but central Asia (60–120°E) stands out as an exception, for which an upward trend can be identified by a portion of the blocking identification methods and time periods used in their study.

The trend of blocking diagnosed with the PV- θ blocking index is higher (and slightly shifted southwards) than the pattern obtained by the AGH_h0 algorithm (Figures 15a,b). As mentioned above, the PV- θ method recognises regions of easterlies that usually lie southwards of blocking highs, which are typically identified by the AGH algorithm. Trend patterns are expected to feature also a meridional shifting, which is obvious in the case of the negative trend in midlatitude BE activity over Europe (Figures 15a,b). When this meridional discrepancy is taken into account, it is evident that the trend pattern obtained by both the PV- θ and the AGH_h0 algorithm present a dipole over Europe. However, in the case that the unmodified AGH algorithm is used, only the southern centre of action is well captured whereas the area of positive trend polewards of Scandinavia is weakly captured. While the AGH_m-10 algorithm can be used for assessing blocking trends in the midlatitudes, the modified algorithm AGH_h0 can be very useful for improving the detection of HLB trends. In particular, the assessment of future blocking trends based on climate model projections can be greatly benefited by a more fitting parametrization of the algorithm in cases where fields of θ on a PV surface are not standard model output; the PV- θ blocking index is then more complex to apply since it would first require computation of PV and interpolation of θ on the 2PVU surface.

6 | DISCUSSION AND CONCLUSIONS

In recent decades, there is increasing interest in understanding the dynamics driving the warming and sea-ice loss trends over the Arctic and the possibility of the Arctic Amplification driving midlatitude cold extremes. Given that blocking is often associated with extremes,

the investigation of the changes in mid- and high-latitude blocking activity has become the centrepiece of the effort to understand the link between the Arctic and midlatitudes. However, the incomplete understanding of blocking dynamics and the plethora of identification methods which often yield differences in the blocking climatology (e.g., Pinheiro *et al.*, 2019) hinder the effort to assess blocking trends. As a notable example, the PV- θ blocking index and the algorithm introduced by D12 disagree on the abundance of HLB activity; the former index yields significantly higher winter blocking activity over Greenland and over Asia, eastwards of the Urals. This study identifies the source of this discrepancy in the addition of the poleward criterion introduced by TM90 and then expanded to 2D by Scherrer *et al.* (2006) and D12. We aim to highlight the need for adopting different algorithm set-ups when the AGH methods are used to identify HLB. Also, the proposed modified algorithm is expected to be a valuable tool which can facilitate the more adequate analysis of HLB in climate model outputs when frequently extensive pre-processing is required for preparing the input variables to the PV- θ blocking index.

Traditionally, absolute field methods identified blocking in areas of easterly flow outbreaks, the most typical characteristic of blocking. Both methods examined here identify blocking as large-scale and persistent reversals of the usual meridional gradient of θ on the dynamical tropopause or geopotential height on the 500 hPa surface. A continuous spectrum of circulation patterns, including blocking highs and cyclones or both (a blocking dipole), can result in blocking and a change of the westerlies to easterlies. The addition of the poleward criterion favours blocking identification at the end of the spectrum featuring blocking highs, whereas a more uniform blocking detection is retained in methods based on the PV- θ blocking index. Both methods yield comparable climatology of BEs in the midlatitudes; the equatorward criterion is indeed the crucial one (as indeed the only criterion in the PV- θ index) for identifying blocking in midlatitudes and, when one occurs, a strong blocking anticyclone is identified which can create an enhanced poleward gradient so that the poleward criterion is usually satisfied.

In contrast, HLB is different because it develops at the northern flanks of the westerlies; it distorts and shifts the westerly jet to the south by wave breaking. This effect can be tested easily by looking only for easterlies. We show that the use of the CT of $-10\text{ m}(\text{°lat})^{-1}$ for the poleward criterion may be appropriate for midlatitudes, but it is too strict for identifying high-latitude BEs. A large proportion of high-latitude events are weak and the associated blocking highs cannot induce poleward gradients and westerlies as strong as in the midlatitudes.

Indeed, a strong zonal westerly flow is not common at very high latitudes and, consequently, many BEs are discarded by the original algorithm introduced by Scherrer *et al.* (2006) and D12. By comparing the PDF of the intensity of the zonal flow in middle and high latitudes, we showed that the use of the value $0 \text{ m}(\text{°lat})^{-1}$ for the CT for latitudes higher than 60°N results in the convergence of the climatology of HLB with that produced by the PV- θ blocking index. We examined the morphology of BEs identified over Greenland and Far East Asia for higher values of the CT, and we confirmed that the added BEs have the typical blocking signature and cannot be dismissed. As the CT approaches zero, blocking anticyclones become weaker and the trough becomes the dominant feature. This corresponds to an increasing proportion of cold-cyclonic rather than warm-cyclonic blocking events being added as the CT threshold increases. These are the cases corresponding to the blocking cyclones probably related to cyclonic wave breaking over the Atlantic where the trough is the dominant feature and the westerlies shift southwards, whereas there are no westerlies at very high latitudes.

We suggest the use of the value $0 \text{ m}(\text{°lat})^{-1}$ for the CT of the poleward criterion, though any slightly lower value could be adopted and yields very similar results (Figure S15). Our suggested choice renders the poleward criterion as a ‘non-easterly’ criterion. In this sense, it retains the traditional character of the method and its propensity to identify blocking highs, though some weaker ones are included. Adoption of slightly positive values for the CT may allow some other very weak high-latitude features to pass through; it then results in a partial or complete elimination of the poleward criterion. Essentially, the elimination of the poleward criterion will render the method nearly equivalent to the blocking index introduced by Masato *et al.* (2013b).

The agreement between the PV- θ blocking index and the algorithm introduced by D12 is higher in the boreal winter and transitional seasons, whereas in summer a zonal asymmetry emerges with the modified AGH algorithms yielding more blocking activity than the PV- θ index eastwards of the Urals and especially over the Bering Strait. The dependence of the blocking climatology on the appropriate cut-off threshold which is in turn sensitive to the spatial (longitudinal and latitudinal) and seasonal variations of the background flow introduces ambiguity to the method, which is not present in methods that make use of the PV- θ index. Parameter tuning in blocking identification methods is always problematic, especially when employed to evaluate blocking in climate model simulations that are characterised by varying model biases.

ACKNOWLEDGEMENTS

The results presented in this study were based on the analysis of ERA-Interim reanalysis data. Information about how to retrieve the ERA-Interim reanalysis from the European Centre for Medium-Range Weather Forecasts (ECMWF) can be found at <https://www.ecmwf.int/en/forecasts/datasets/archive-datasets/reanalysis-datasets/era-interim> (accessed 28 December 2020). The research leading to these results has received funding from the German Federal Ministry of Education and Research (BMBF) through the JPI Climate/Belmont Forum Inter-Dec project (FKZ: 01LP1609A; ET, DM, JB, EM), JPI Climate/JPI Oceans NextG-Climate Science-ROADMAP (FKZ: 01LP2002A; ET, DM, JB, EM) and from the EU H2020 Blue-Action (GA 727852; EM, ET and DM). The authors wish to thank Professor Brian Hoskins for his very constructive comments on the results and Dr. Chao Li for a comprehensive internal review of the manuscript. Open Access funding enabled and organized by ProjektDEAL.

ORCID

Evangelos Tyrlis  <https://orcid.org/0000-0002-0423-4926>

REFERENCES

- Athanasiadis, P.J., Yeager, S., Kwon, Y.-O., Belluci, A., Smith, D.W. and Tibaldi, S. (2020) Decadal predictability of North Atlantic blocking and the NAO. *npj Climate and Atmospheric Science*, 3. <https://doi.org/10.1038/s41612-020-0120-6>.
- Ballinger, T.J., Hanna, E., Hall, R.J., Cropper, T.E., Miller, J., Ribergaard, M., Overland, J.E. and Høyer, J.L. (2018) Anomalous blocking over Greenland preceded the 2013 extreme early melt of local sea ice. *Annals of Glaciology*, 59, 181–190. <https://doi.org/10.1017/aog.2017.30>.
- Barnes, E.A. (2013) Revisiting the evidence linking Arctic amplification to extreme weather in midlatitudes. *Geophysical Research Letters*, 40, 4734–4739. <https://doi.org/10.1002/grl.50880>.
- Barnes, E.A., Slingo, J. and Woollings, T.J. (2012) A methodology for the comparison of blocking climatologies across indices, models and climate scenarios. *Climate Dynamics*, 38, 2467–2481. <https://doi.org/10.1007/s00382-011-1243-6>.
- Barnes, E.A., Dunn-Sigouin, E., Masato, G. and Woollings, T.J. (2014) Exploring recent trends in Northern Hemisphere blocking. *Geophysical Research Letters*, 41, 638–644. <https://doi.org/10.1002/2013GL058745>.
- Barriopedro, D., Fischer, E.M., Luterbacher, J., Trigo, R.M. and García-Herrera, R. (2011) The hot summer of 2020: redrawing the temperature record map of Europe. *Science*, 332, 220–224. <https://doi.org/10.1126/science.1201224>.
- Barriopedro, P., García-Herrera, R. and Trigo, R.M. (2010) Application of blocking diagnosis methods to general circulation models. Part I: a novel detection scheme. *Climate Dynamics*, 35, 1373–1391. <https://doi.org/10.1007/s00382-010-0767-5>.
- Berggren, R., Bolin, B. and Rossby, C.-G. (1949) An aerological study of zonal motion, its perturbations and break-down. *Tellus*, 1(2), 14–37. <https://doi.org/10.1111/j.2153-3490.1949.tb01257.x>.

- Berrisford, P., Hoskins, B.J. and Tyrlis, E. (2007) Blocking and Rossby wave breaking on the dynamical tropopause in the Southern Hemisphere. *Journal of the Atmospheric Sciences*, 64, 2881–2898. <https://doi.org/10.1175/JAS3984.1>.
- Bieli, M., Pfahl, S. and Wernli, H. (2015) A Lagrangian investigation of hot and cold temperature extremes in Europe. *Quarterly Journal of the Royal Meteorological Society*, 151, 98–108. <https://doi.org/10.1002/qj.2339>.
- Black, E., Blackburn, M., Harrison, G., Hoskins, B.J. and Methven, J. (2004) Factors contributing to the summer 2003 European heatwave. *Weather*, 59, 217–223. <https://doi.org/10.1256/wea.74.04>.
- Buehler, T., Raible, C.C. and Stocker, T.F. (2010) The relationship of winter season North Atlantic blocking frequencies to extreme cold or dry spells in the ERA-40. *Tellus, Series A*, 63A, 212–222. <https://doi.org/10.1111/j.1600-0870.2010.00492.x>.
- Charney, J.G., Shukla, J. and Mo, K.C. (1981) Comparison of a barotropic blocking theory with observation. *Journal of the Atmospheric Sciences*, 38, 762–779. [https://doi.org/10.1175/1520-0469\(1981\)038<0762:COABBT>2.0.CO;2](https://doi.org/10.1175/1520-0469(1981)038<0762:COABBT>2.0.CO;2).
- Chen, X., Luo, D., Feldstein, S.B. and Lee, S. (2018) Impact of winter Ural blocking on Arctic sea ice: short-time variability. *Journal of Climate*, 31, 2267–2282. <https://doi.org/10.1175/JCLI-D-17-0194.1>.
- Cohen, J., Zhang, X., Francis, J., Jung, T., Kwok, R., Overland, J., Ballinger, T.J., Bhatt, U.S., Chen, H.W., Coumou, D., Feldstein, S., Gu, H., Handorf, D., Henderson, G., Ionita, M., Kretschmer, M., Laliberte, F., Lee, S., Linderholm, H.W., Maslowski, W., Peings, Y., Pfeiffer, K., Rigor, I., Semmler, T., Stroeve, J., Taylor, P.C., Vavrus, S., Vihma, T., Wang, S., Wendisch, M., Wu, Y. and Yoon, J. (2020) Divergent consensus on Arctic amplification influence on midlatitude severe winter weather. *Nature Climate Change*, 10, 20–29. <https://doi.org/10.1038/s41558-019-0662-y>.
- Croci-Maspoli, M., Schwierz, C. and Davies, H.C. (2007) A multifaceted climatology of atmospheric blocking and its recent linear trend. *Journal of Climate*, 20, 633–649. <https://doi.org/10.1175/JCLI4029.1>.
- Davini, P., Cagnazzo, C., Gualdi, S. and Navarra, A. (2012) Bidimensional diagnostics, variability, and trends of Northern Hemisphere blocking. *Journal of Climate*, 25, 6496–6509. <https://doi.org/10.1175/JCLI-D-12-00032.1>.
- Davini, P., Cagnazzo, C. and Anstey, J.A. (2014) A blocking view of the stratosphere–troposphere coupling. *Journal of Geophysical Research*, 119, 11100–11115. <https://doi.org/10.1002/2014JD021703>.
- Davini, P., Corti, S., D’Andrea, F., Rivière, G. and von Hardenberg, J. (2017) Improved winter European atmospheric blocking frequencies in high-resolution global climate simulations. *Journal of Advances in Modeling Earth Systems*, 9, 2615–2634. <https://doi.org/10.1002/2017MS001082>.
- Dee, D.P., Uppala, S.M., Simmons, A.J., Berrisford, P., Poli, P., Kobayashi, S., Andrae, U., Balmaseda, M.A., Balsamo, G., Bauer, P., Bechtold, P., Beljaars, A.C.M., van de Berg, L., Bidlot, J., Bormann, N., Delsol, C., Dragani, R., Fuentes, M., Geer, A.J., Haimberger, L., Healy, S.B., Hersbach, H., Hólm, E.V., Isaksen, I., Kållberg, P., Köhler, M., Matricardi, M., McNally, A.P., Monge-Sanz, B.M., Morcrette, J.-J., Park, B.-K., Peubey, C., de Rosnay, P., Tavolato, C., Thépaut, J.-N. and Vitart, F. (2011) The ERA-Interim reanalysis: configuration and performance of the data assimilation system. *Quarterly Journal of the Royal Meteorological Society*, 137, 553–597. <https://doi.org/10.1002/qj.828>.
- Ding, Q., Schweiger, A., L’Heureux, M., Battisti, D.S., Po-Chedley, S., Johnson, N.C., Blanchard-Wrigglesworth, E., Harnos, K., Zhang, Q., Eastman, R. and Steig, E.J. (2017) Influence of high-latitude atmospheric circulation changes on summertime Arctic sea ice. *Nature*, 7, 289–296. <https://doi.org/10.1038/NCLIMATE3241>.
- Dole, R., Hoerling, M., Perlwitz, J., Eischeid, J., Pegion, P., Zhang, T., Quan, X.-W., Xu, T. and Murray, D. (2011) Was there a basis for anticipating the 2010 Russian heat wave?. *Geophysical Research Letters*, 38. <https://doi.org/10.1029/2010GL046582>.
- Dole, R.M. (1986) Persistent anomalies of the extratropical Northern Hemisphere wintertime circulation: structure. *Monthly Weather Review*, 114, 178–207. [https://doi.org/10.1175/1520-0493\(1986\)114<0178:PAOTEN>2.0.CO;2](https://doi.org/10.1175/1520-0493(1986)114<0178:PAOTEN>2.0.CO;2).
- Dole, R.M. and Gordon, N.D. (1983) Persistent anomalies of the extratropical Northern Hemisphere wintertime circulation: geographical distribution and regional persistence characteristics. *Monthly Weather Review*, 111, 1567–1586. [https://doi.org/10.1175/1520-0493\(1983\)111<1567:PAOTEN>2.0.CO;2](https://doi.org/10.1175/1520-0493(1983)111<1567:PAOTEN>2.0.CO;2).
- Dunn-Sigouin, E., Son, S.-W. and Lin, H. (2013) Evaluation of Northern Hemisphere blocking climatology in the global environment multiscale model. *Monthly Weather Review*, 141, 707–727. <https://doi.org/10.1175/MWR-D-12-00134.1>.
- Elliott, R.D. and Smith, T.B. (1949) A study of the effects of large blocking highs on the general circulation in the Northern Hemisphere westerlies. *Journal of Meteorology*, 6, 67–85. [https://doi.org/10.1175/1520-0469\(1949\)006<0068:ASOTEO>2.0.CO;2](https://doi.org/10.1175/1520-0469(1949)006<0068:ASOTEO>2.0.CO;2).
- Francis, J.A. and Vavrus, S.J. (2012) Evidence linking Arctic amplification to extreme weather in mid-latitudes. *Geophysical Research Letters*, 39, L06801. <https://doi.org/10.1029/2012GL051000>.
- Francis, J.A. and Vavrus, S.J. (2015) Evidence for a wavier jet stream in response to rapid Arctic warming. *Environmental Research Letters*, 10. <https://doi.org/10.1088/1748-9326/10/1/014005>.
- Gabriel, A. and Peters, D. (2008) A diagnostic study of different types of Rossby wave breaking events in the Northern Extratropics. *Journal of the Meteorological Society of Japan*, 86, 613–631. <https://doi.org/10.2151/jmsj.86.613>.
- Garfinkel, C.I., Son, S.-W., Song, K., Aquila, V. and Oman, L.D. (2017) Stratospheric variability contributed to and sustained the recent hiatus in Eurasian winter warming. *Geophysical Research Letters*, 44, 374–382. <https://doi.org/10.1002/2016GL072035>.
- Gong, T. and Luo, D. (2017) Ural blocking as an amplifier of the Arctic sea ice decline in winter. *Journal of Climate*, 30, 2639–2654. <https://doi.org/10.1175/JCLI-D-16-0548.1>.
- Green, J.S.A. (1977) The weather during July 1976: some dynamical consideration of the drought. *Weather*, 32, 120–126. <https://doi.org/10.1002/j.1477-8696.1977.tb04532.x>.
- Hermann, M., Papritz, L. and Wernli, H. (2020) A Lagrangian analysis of the dynamical and thermodynamic drivers of Greenland melt events during 1979–2017. *Weather Climate Dynamics*, 1, 497–518. <https://doi.org/10.5194/wcd-1-497-2020>.
- Hoskins, B.J., McIntyre, M.E. and Robertson, A.W. (1985) On the use and significance of isentropic potential vorticity maps. *Quarterly Journal of the Royal Meteorological Society*, 111, 877–946. <https://doi.org/10.1002/qj.49711147002>.
- Huang, J., Tian, W., Zhang, J., Huang, Q., Tian, H. and Luo, J. (2017) The connection between extreme stratospheric polar vortex events and tropospheric blockings. *Quarterly Journal of the*

- Royal Meteorological Society*, 143, 1148–1164. <https://doi.org/10.1002/qj.3001>.
- King, A.D., Butler, A.H., Jucker, M., Earl, N.O. and Rudeva, I. (2019) Observed relationships between sudden stratospheric warmings and European climate extremes. *Journal of Geophysical Research*, 124, 13943–13961. <https://doi.org/10.1029/2019JD030480>.
- Knox, J.L. and Hay, J.E. (1985) Blocking signatures in the Northern Hemisphere: frequency distribution and interpretation. *Journal of Climatology*, 5, 1–16. <https://doi.org/10.1002/joc.3370050102>.
- Kostad, E.W., Breiteig, T. and Scaife, A.A. (2010) The association between stratospheric weak polar vortex events and cold air outbreaks in the Northern Hemisphere. *Quarterly Journal of the Royal Meteorological Society*, 136, 886–893. <https://doi.org/10.1002/qj.620>.
- Kretschmer, M., Coumou, D., Agel, L., Barlow, M., Tziperman, E. and Cohen, J. (2018) More-persistent weak stratospheric polar vortex states linked to cold extremes. *Bulletin of the American Meteorological Society*, 99, 49–60. <https://doi.org/10.1175/BAMS-D-16-0259.1>.
- Lau, W.K.M. and Kim, K.-M. (2012) The 2012 Pakistan flood and Russian heat wave: teleconnection of hydrometeorological extremes. *Journal of Hydrometeorology*, 13, 392–403. <https://doi.org/10.1175/JHR-D-11-016.1>.
- Lee, S., Gong, T., Feldstein, S.B., Screen, J.A. and Simmonds, I. (2017) Revisiting the cause of the 1989–2009 Arctic surface warming using the surface energy budget: downward infrared radiation dominates the surface fluxes. *Geophysical Research Letters*, 44, 10654–10661. <https://doi.org/10.1002/2017GL075375>.
- Lehtonen, I. and Karpechko, A.Y. (2016) Observed and modeled tropospheric cold anomalies associated with sudden stratospheric warmings. *Journal of Geophysical Research*, 121, 1591–1610. <https://doi.org/10.1002/2015JD023860>.
- Lenggenhager, S., Croci-Maspoli, M., Brönnimann, S. and Martius, O. (2019) On the dynamical coupling between atmospheric blocks and heavy precipitation events: a discussion of the southern Alpine flood in October 2000. *Quarterly Journal of the Royal Meteorological Society*, 145, 530–545. <https://doi.org/10.1002/qj.3449>.
- Luo, D., Xiao, Y., Yao, Y., Dai, A., Simmonds, I. and Franzke, C.L.E. (2016) Impact of Ural blocking on winter warm Arctic–cold Eurasian anomalies. Part I: blocking induced amplification. *Journal of Climate*, 29, 3925–3947. <https://doi.org/10.1175/JCLI-D-15-0611.1>.
- Luo, D., Yao, Y., Dai, A., Simmonds, I. and Zhong, L. (2017) Increased quasi-stationarity and persistence of winter Ural blocking and Eurasian extreme cold events in response to Arctic warming. Part II: A theoretical explanation. *Journal of Climate*, 30, 3569–3587. <https://doi.org/10.1175/JCLI-D-16-0262.1>.
- Luo, D., Chen, X., Overland, I., Simmonds, I., Wu, Y. and Zhang, P. (2019) Weakened potential vorticity barrier linked to recent winter Arctic sea ice loss and midlatitude cold extremes. *Journal of Climate*, 32, 4235–4261. <https://doi.org/10.1175/JCLI-D-18-0449.1>.
- Martius, O., Polvani, L.M. and Davies, H.C. (2009) Blocking precursors to stratospheric sudden warming events. *Geophysical Research Letters*, 36. <https://doi.org/10.1029/2009GL038776>.
- Martius, O., Sodemann, H., Joos, H., Pfahl, S., Winschall, A., Croci-Maspoli, M., Graf, M., Madonna, E., Mueller, B., Schemm, S., Sedláček, J., Sprenger, M. and Wernli, H. (2013) The role of upper-level dynamics and surface processes for the Pakistan flood of July 2010. *Quarterly Journal of the Royal Meteorological Society*, 139, 1780–1797. <https://doi.org/10.1002/qj.2082>.
- Masato, G., Hoskins, B.J. and Woollings, T.J. (2009) Can the frequency of blocking be described by a red noise process?. *Journal of the Atmospheric Sciences*, 66, 2143–2149. <https://doi.org/10.1175/2008JAS2907.1>.
- Masato, G., Hoskins, B.J. and Woollings, T.J. (2012) Wavebreaking characteristics of midlatitude blocking. *Quarterly Journal of the Royal Meteorological Society*, 138, 1285–1296. <https://doi.org/10.1002/qj.990>.
- Masato, G., Hoskins, B.J. and Woollings, T.J. (2013a) Wave-breaking characteristics of Northern Hemisphere winter blocking: a two-dimensional approach. *Journal of Climate*, 26, 4535–4549. <https://doi.org/10.1175/JCLI-D-12-00240.1>.
- Masato, G., Hoskins, B.J. and Woollings, T.J. (2013b) Winter and summer Northern Hemisphere blocking in CMIP5 models. *Journal of Climate*, 26, 7044–7059. <https://doi.org/10.1175/JCLI-D-12-00466.1>.
- Matsueda, M. (2011) Predictability of Euro-Russian blocking in summer of 2010. *Geophysical Research Letters*, 38. <https://doi.org/10.1029/2010GL046557>.
- McLeod, J.T. and Mote, T.L. (2016) Linking interannual variability in extreme Greenland blocking episodes to the recent increase in summer melting across the Greenland ice sheet. *International Journal of Climatology*, 36, 1484–1499. <https://doi.org/10.1002/joc.4440>.
- Mori, M., Watanabe, M., Shiogama, H., Inoue, J. and Kimoto, M. (2014) Robust Arctic sea-ice influence on the frequent Eurasian cold winters in past decades. *Nature Geosciences*, 7, 869–873. <https://doi.org/10.1038/ngeo2277>.
- Mori, M., Kosaka, Y., Watanabe, M., Nakamura, H. and Kimoto, M. (2019) A reconciled estimate of the influence of Arctic sea-ice loss on recent Eurasian cooling. *Nature Climate Change*, 9, 123–129. <https://doi.org/10.1038/s41558-018-0379-3>.
- Nabizadeh, E., Hassanzadeh, P., Yang, D. and Barnes, E.A. (2019) Size of the atmospheric blocking events: scaling law and response to climate change. *Geophysical Research Letters*, 46, 13488–13499. <https://doi.org/10.1029/2019GL084863>.
- Nakamura, N. and Huang, C.S.Y. (2018) Atmospheric blocking as a traffic jam in the jet stream. *Science*, 361, 42–47. <https://doi.org/10.1126/science.aat0721>.
- Nishii, K., Nakamura, H. and Orsolini, Y.J. (2011) Geographical dependence observed in blocking high influence on the stratospheric variability through enhancement and suppression of upward planetary-wave propagation. *Journal of Climate*, 24, 6408–6423. <https://doi.org/10.1175/JCLI-D-10.05021.1>.
- Ogi, M. and Wallace, J.M. (2012) The role of summer surface wind anomalies in the summer Arctic sea ice extent in 2010 and 2011. *Geophysical Research Letters*, 39. <https://doi.org/10.1029/2012GL051330>.
- Overland, J.E., Francis, J.A., Hanna, E. and Wang, W. (2012) The recent shift in early summer Arctic atmospheric circulation. *Geophysical Research Letters*, 39. <https://doi.org/10.1029/2012GL053268>.
- Papritz, L. and Wernli, H. (2018) Role of polar anticyclones and mid-latitude cyclones for Arctic summertime sea-ice melting. *Nature Geosciences*, 11, 108–113. <https://doi.org/10.1038/s41561-017-0041-0>.

- Peings, Y. (2019) Ural blocking as a driver of early-winter stratospheric warmings. *Geophysical Research Letters*, 46, 5460–5468. <https://doi.org/10.1029/2019GL082097>.
- Pelly, J. and Hoskins, B.J. (2003) A new perspective on blocking. *Journal of the Atmospheric Sciences*, 60, 743–755. [https://doi.org/10.1175/1520-0469\(2003\)060<0743:ANPOB>2.0.CO;2](https://doi.org/10.1175/1520-0469(2003)060<0743:ANPOB>2.0.CO;2).
- Peters, D. and Waugh, D.W. (1996) Influence of barotropic shear on the poleward advection of upper-tropospheric air. *Journal of the Atmospheric Sciences*, 53, 3013–3031. [https://doi.org/10.1175/1520-0469\(1996\)053<3013:IOBSOT>2.0.CO;2](https://doi.org/10.1175/1520-0469(1996)053<3013:IOBSOT>2.0.CO;2).
- Pinheiro, M.C., Ullrich, P.A. and Grotjahn, R. (2019) Atmospheric blocking and intercomparison of objective detection methods: flow field characteristics. *Climate Dynamics*, 53, 4189–4216. <https://doi.org/10.1007/s00382-019-04782-5>.
- Rex, D.F. (1950) Blocking action in the middle troposphere and its effect on regional climate. I: an aerological study of blocking action. *Tellus*, 2(3), 196–211. <https://doi.org/10.1111/j.2153-3490.1950.tb00331.x>.
- Scherrer, S.C., Croci-Maspoli, M., Schwierz, C. and Appenzeller, C. (2006) Two-dimensional indices of atmospheric blocking and their statistical relationship with winter climate patterns in the Euro-Atlantic region. *International Journal of Climatology*, 26, 233–249. <https://doi.org/10.1002/joc.1250>.
- Schiemann, R., Athanasiadis, P., Barriopedro, D., Doblas-Reyes, F., Lohmann, K., Roberts, M.J., Sein, D.V., Roberts, C.D., Terray, L. and Vidale, P.L. (2020) Northern Hemisphere blocking simulation in current climate models: evaluating progress from the Climate Model Intercomparison Project Phase 5 to 6 and sensitivity to resolution. *Weather Climate Dynamics*, 1, 277–292. <https://doi.org/10.5194/wcd-1-277-2020>.
- Schneider, A., Schubert, S., Vargin, P., Lunkeit, F., Zhu, X., Peters, D.H.W. and Fraedrich, K. (2012) Large-scale flow and the long-lasting blocking high over Russia: summer 2010. *Monthly Weather Review*, 140, 2967–2981. <https://doi.org/10.1175/MWR-D-11-00249.1>.
- Schwierz, C., Croci-Maspoli, M. and Davies, H.C. (2004) Perspicacious indicators of atmospheric blocking. *Geophysical Research Letters*, 31. <https://doi.org/10.1029/2003GL019341>.
- Serreze, M.C. and Francis, J.A. (2006) The Arctic amplification debate. *Climatic Change*, 76, 241–264. <https://doi.org/10.1007/s10584-005-9017-y>.
- Shukla, J. and Mo, K.C. (1983) Seasonal and geographical variation of blocking. *Monthly Weather Review*, 111, 388–402. [https://doi.org/10.1175/1520-0493\(1983\)111<0388:SAGVOB>2.0.CO;2](https://doi.org/10.1175/1520-0493(1983)111<0388:SAGVOB>2.0.CO;2).
- Sillmann, J. and Croci-Maspoli, M. (2009) Present and future atmospheric blocking and its impact on European mean and extreme climate. *Geophysical Research Letters*, 36. <https://doi.org/10.1029/2009GL038259>.
- Sprenger, M., Fragkoulidis, G., Binder, H., Croci-Maspoli, M., Graf, P., Grams, C.M., Knippertz, P., Madonna, E., Schemm, S., Škerlak, B. and Wernli, H. (2017) Global climatologies of Eulerian and Lagrangian flow features based on ERA-Interim. *Bulletin of the American Meteorological Society*, 98, 1739–1748. <https://doi.org/10.1175/BAMS-D-15-00299.1>.
- Steinfeld, D. and Pfahl, S. (2019) The role of latent heating in atmospheric blocking dynamics: a global climatology. *Climate Dynamics*, 53, 6159–6180. <https://doi.org/10.1007/s00382-019-04919-6>.
- Sun, L., Perlwitz, J. and Hoerling, M. (2016) What caused the recent “Warm Arctic, Cold Continents” trend pattern in winter temperatures?. *Geophysical Research Letters*, 43, 5345–5352. <https://doi.org/10.1002/2016GL069024>.
- Takaya, K. and Nakamura, H. (2005) Geographical dependence of upper-level blocking formation associated with intraseasonal amplification of the Siberian high. *Journal of the Atmospheric Sciences*, 62, 4441–4449. <https://doi.org/10.1175/JAS3628.1>.
- Thorncroft, C.D., Hoskins, B.J. and McIntyre, M.E. (1993) Two paradigms of baroclinic-wave life-cycle behaviour. *Quarterly Journal of the Royal Meteorological Society*, 119, 17–55. <https://doi.org/10.1002/qj.49711950903>.
- Tibaldi, S. and Molteni, F. (1990) On the operational predictability of blocking. *Tellus, series A*, 42A, 343–365. <https://doi.org/10.1034/j.1600-0870.1990.t01-2-00003.x>.
- Treidl, R.A., Birch, E.C. and Sajecki, P. (1981) Blocking action in the Northern Hemisphere: a climatological study. *Atmosphere–Ocean*, 19, 1–23. <https://doi.org/10.1080/07055900.1981.9649096>.
- Trigo, R.M., Garcia-Herrera, R., Diaz, J. and Trigo, I.F. (2005) How exceptional was the early August 2003 heatwave in France?. *Geophysical Research Letters*, 32. <https://doi.org/10.1029/2005GL022410>.
- Tyrlis, E. and Hoskins, B.J. (2008a) Aspects of a Northern Hemisphere atmospheric blocking climatology. *Journal of the Atmospheric Sciences*, 65, 1638–1652. <https://doi.org/10.1175/2007JAS2337.1>.
- Tyrlis, E. and Hoskins, B.J. (2008b) The morphology of Northern Hemisphere blocking. *Journal of the Atmospheric Sciences*, 65, 1653–1665. <https://doi.org/10.1175/2007JAS2338.1>.
- Tyrlis, E., Tymvios, F.S., Giannakopoulos, C. and Lelieveld, J. (2015) The role of blocking in the summer 2014 collapse of Etesians over the Eastern Mediterranean. *Journal of Geophysical Research*, 120, 6777–6792. <https://doi.org/10.1002/2015JD023543>.
- Tyrlis, E., Manzini, E., Bader, J., Ukita, J., Nakamura, H. and Matei, D. (2019) Ural blocking driving extreme Arctic sea ice loss, cold Eurasia, and stratospheric vortex weakening in autumn and early winter 2016–2017. *Journal of Geophysical Research*, 124, 11313–11329. <https://doi.org/10.1029/2019JD031085>.
- Tyrlis, E., Bader, J., Manzini, E., Ukita, J., Nakamura, H. and Matei, D. (2020) On the role of Ural blocking in driving the Warm Arctic–Cold Siberia pattern. *Quarterly Journal of the Royal Meteorological Society*, 146, 2138–2153. <https://doi.org/10.1002/qj.3784>.
- Wang, S., Nath, D., Chen, W. and Wang, L. (2019) Recent strengthening of Greenland blocking drives summertime surface warming over northern Canada and Eastern Siberia. *Journal of Climate*, 32, 3263–3278. <https://doi.org/10.1175/JCLI-D-18-0410.1>.
- Webster, P.J., Toma, V.E. and Kim, H.-M. (2011) Were the 2010 Pakistan floods predictable?. *Geophysical Research Letters*, 38. <https://doi.org/10.1029/2010GL046346>.
- Whan, K., Zwiers, F. and Sillman, J. (2016) The influence of atmospheric blocking on extreme winter minimum temperatures in North America. *Journal of Climate*, 29, 4361–4381. <https://doi.org/10.1175/JCLI-D-15-0493.1>.
- White, I., Garfinkel, C.I., Gerber, E.P., Jucker, M., Aquila, V. and Oman, L.D. (2019) The downward influence of sudden stratospheric warmings: association with tropospheric precursors. *Journal of Climate*, 32, 85–108. <https://doi.org/10.1175/JCLI-D-18-0053.1>.

- Witze, A. (2019) Dramatic sea-ice melt caps tough Arctic summer. *Nature*, 573, 320–321. <https://doi.org/10.1038/d41586-019-02653-x>.
- Woods, C. and Caballero, R. (2013) The role of moist intrusions in winter Arctic warming and sea ice decline. *Journal of Climate*, 29, 4473–4485. <https://doi.org/10.1175/JCLI-D-15-0773.1>.
- Woods, C., Caballero, R. and Svensson, G. (2013) Large-scale circulation associated with moisture intrusions into the Arctic during winter. *Geophysical Research Letters*, 40, 4717–4121. <https://doi.org/10.1002/grl.50912>.
- Woollings, T.J., Hoskins, B.J., Blackburn, P. and Berrisford, P. (2008) A new Rossby wave-breaking interpretation of the North Atlantic Oscillation. *Journal of the Atmospheric Sciences*, 65, 609–626. <https://doi.org/10.1175/2007JAS2347.1>.
- Woollings, T.J., Charlton-Perez, A., Ineson, S., Marshall, A.G. and Masato, G. (2010) Associations between stratospheric variability and tropospheric blocking. *Journal of Geophysical Research*, 115. <https://doi.org/10.1002/2009JD012742>.
- Woollings, T.J., Barriopedro, D., Methven, J., Son, S.-W., Martius, O., Harvey, B., Sillmann, J., Lupo, A.R. and Seneviratne, S. (2018) Blocking and its response to climate change. *Current Climate*

Change Reports, 4, 287–300. <https://doi.org/10.1007/s40641-018-0108-z>.

- Yao, Y., Luo, D., Dai, A. and Simmonds, I. (2017) Increased quasi-stationarity and persistence of winter Ural blocking and Eurasian extreme cold events in response to Arctic warming. Part I: insights from observational analyses. *Journal of Climate*, 30, 3549–3568. <https://doi.org/10.1175/JCLI-D-16-0261.1>.

SUPPORTING INFORMATION

Additional supporting information may be found online in the Supporting Information section at the end of this article.

How to cite this article: Tyrlis E, Bader J, Manzini E, Matei D. Reconciling different methods of high-latitude blocking detection. *Q.J.R. Meteorol. Soc.* 2021;1–27. <https://doi.org/10.1002/qj.3960>